Table 2. Demographic and clinical characteristics of Responders and Non-responders

	Responders (n=7) Mean (SD)	Non-responders (n=4) Mean (SD)	p
Age, years	70.7 (8.2)	74.5 (3.8)	0.296
Gender (% female)	85.7	50.0	-
Onset, years	69.7 (8.4)	73.8 (4.0)	0.257
Family history of dementia (%)	42.9	25.0	-
Duration of dementia, years	1.2 (0.8)	0.9 (0.7)	0.392
Education, years	9.0 (3.3)	8.8 (1.5)	0.360
HDS-R	19.6 (6.0)	15.8 (3.5)	0.256
ADAS-J cog pre	18.7 (8.1)	17.3 (11.5)	1.000
post	12.5 (7.4)	21.6 (11.4)	0.107

HDS-R, the Revised Hasegawa Dementia Scale; and ADAS-J cog, the Japanese version of the Alzheimer's disease Assessment Scale cognitive subscale.

Table 3. The total scores of ADAS-J cog and the ratios of uptake in each lobe to that in the cerebellum in each patient

		gender	age	HDS-R	ADAS-J cog total score		the ratios of each lobe to the cerebellum									
							frontal		temporal		occipital		parietal		temporoparietal	
					before	after	before	after	before	after	before	after	before	after	before	after
Responders	case1	male	66	19	13.7	11.7	0.64	0.82	0.83	0.86	1.1	0.97	1.03	1.05	1.1	0.97
	case2	female	70	21	19	9	0.22	0.92	0.69	1.03	0.74	1.28	1.25	1.03	0.74	1.28
	case3	female	63	26	12.7	6.7	0.27	1.22	0.28	1.11	0.77	1.22	1.44	1.11	0.77	1.22
	case4	female	61	24	11	6.4	1.02	1	1.02	1.14	1.38	1.31	0.85	1	1.38	1.31
	case5	female	76	24	14.7	11	0.92	0.96	0.98	0.99	1.09	1.08	0.78	0.79	0.97	0.97
	case6	female	75	13	29.7	14.4	0.26	0.64	0.3	0.57	0.75	0.9	0.9	2.02	0.96	0.67
	case7	female	84	10	30.3	28	0.59	0.47	1.12	0.91	1.11	0.82	1.18	0.94	0.77	0.58
	the average of the ratio (SD)*1						2.18 (1.58)		1.62 (1.10)		1.15 (0.37)		1.12 (0.52)		1.09 (0.41)	
Non-responders	case8	male	69	14	33.3	33	0.98	0.2	0.91	0.58	0.97	0.64	0.89	1.1	0.97	0.64
	case9	female	77	17	15.6	15	1.15	1.12	1.1	0.93	1.47	1.15	1.04	0.97	1.47	1.15
	case10	female	77	12	6	9	0.99	0.92	0.97	0.99	1.35	1.28	1.06	0.95	1.13	1.21
	case11	male	75	20	14.4	29.3	1.24	0.81	1.19	1.23	1.33	0.8	1.18	1.03	1.14	0.25
	the average of the ratio (SD)*1						0.69 (0.35)		0.88 (0.19)		0.75 (0.15)		0.98 (0.17)		0.68 (0.35)	
	p						0.023*2		0.089		0.038*2		0.850		0.186	

HDS-R, the Revised Hasegawa Dementia Scale; and ADAS-J cog, the Japanese version of the Alzheimer's disease Assessment Scale cognitive subscale. *1, the average of the ratio of the mean count after treatment to the count before treatment; and *2, $p<0.05$.

patients showed typical pattern for Alzheimer's disease on PET images and significant regional CBF reduction in the posterior cingulate gyrus and/or precuneus region on SPECT images using eZIS.

The ratios of the mean post-treatment uptake to the pre-treatment uptake in five bilateral pairs of ROIs on portions of each lobe are shown in Figure 2. Table 3 shows the total scores of ADAS-J cog and the ratios of uptake in each lobe to that in the cerebellum in each patient. In Responders, the averages of the ratios of the mean counts after treatment to the counts pre-

treatment in the frontal, temporal, occipital, parietal, and temporoparietal lobes were 2.18, 1.62, 1.15, 1.12, and 1.09 respectively, while those in the Non-responders were 0.69, 0.88, 0.75, 0.98, and 0.68 respectively (Table 3). In the frontal and occipital lobes, the Responders showed significantly increased glucose metabolism compared with that in Non-responders ($p<0.05$) (Fig. 2).

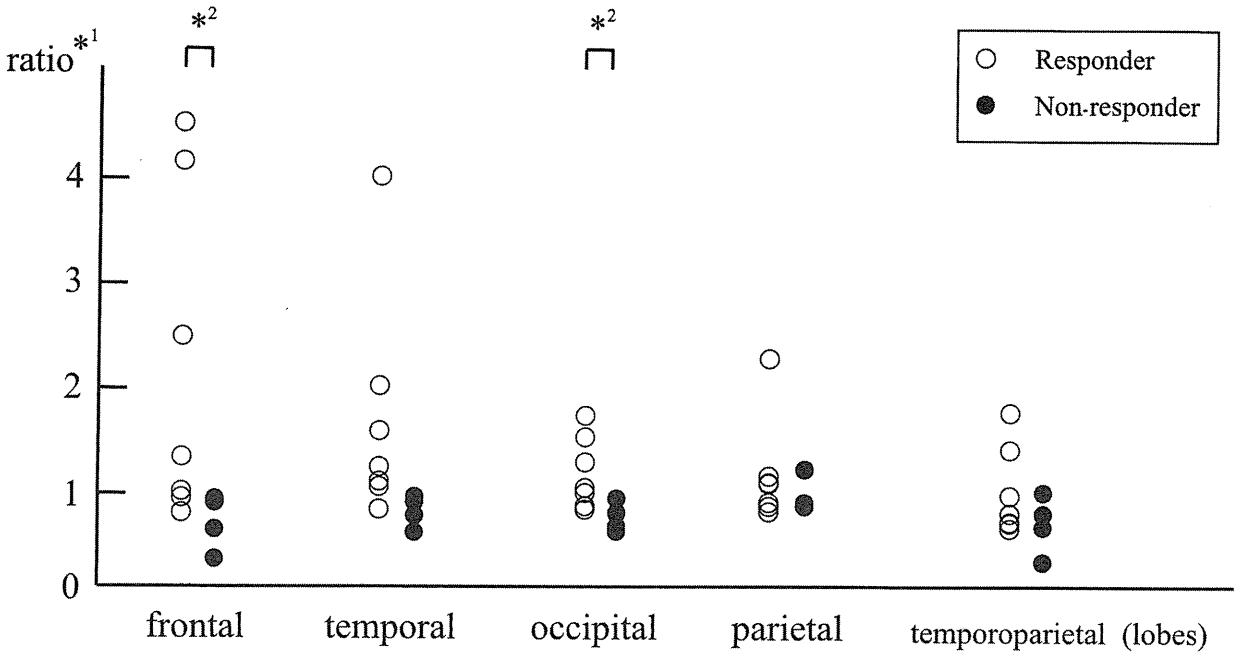

Figure 2. The ratios of the mean post-treatment uptake to the pre-treatment uptake in five bilateral pairs of ROIs on portions of each lobe. *1, the ratio of the mean count after treatment to the count before treatment; and *2, $p<0.05$.

Discussion

We attempted to evaluate the therapeutic response to Donepezil in patients with DAT using FDG-PET in this study. After treatment, Responders showed increased FDG uptake in the frontal, temporal, and occipital lobes on average. Non-responders showed decreased uptake in the frontal, temporal, occipital, and temporoparietal lobes. These findings suggest that the therapeutic response to Donepezil could be evaluated by measuring glucose metabolism in brain regions using FDG-PET.

Short-term treatment with different AChEIs such as Tacrine, Donepezil, Physostigmine, Metrifonate, Rivastigmine, and Galantamine have shown an increase in CBF or glucose metabolism in patients with DAT[4,5,11,18-20]. Especially, frontal metabolism or CBF increase during AChEIs treatment has often been reported[4,5,11]. In this study, we also found a marked increase in glucose metabolism especially in the frontal lobes of Responders. This finding is consistent with the findings of previous PET studies regarding AChEIs treatment. Tune et al also evaluated the effects of 24 weeks Donepezil treatment on regional glucose metabolism in the patients with DAT by using ROI analysis[13]. They reported that significant treatment differences for the mean percentage change from baseline in regional brain glucose metabolism were observed in the right parietal lobe and left temporal lobe in addition to bilateral frontal lobe. These results may have varied with differences in the duration of the treatment, the dose or the use of different reference

region in the ROI method. We evaluated the therapeutic response at 12 weeks because the Japanese clinical research on Donepezil therapy revealed that significant differences were found after 12 weeks of the treatment between Donepezil and placebo groups[16]. However, some studies on AChEIs suggested the difference became statistically significant after 24 weeks treatment[2,3,13]. Therefore we also have to make further investigation about 24 weeks treatment to clarify the effect of the Donepezil therapy.

At present, a cognitive performance test such as the Alzheimer's disease Assessment Scale cognitive subscale[16,19,21] or the Mini-Mental State Examination is used to monitor the response to AChEIs[4,22]. However, the result of these tests may be influenced by the subjective judgment of the examiner and the mental condition of the patient, such as depressive mood, hallucination or delusion. Therefore, we designed this study to find a method that would facilitate evaluation of therapeutic response in patients with DAT regardless of clinical symptoms.

Functional neuroimaging methods (such as SPECT or PET) are widely used in the early diagnosis of DAT because reduced CBF and metabolism in patients with DAT is typically observed in the temporoparietal brain region and posterior cingulate cortex[8]. DAT patients can undergo PET in a resting state without mental task and the data are not influenced by the patient's transient level of motivation or physical condition. Particularly, FDG-PET provides more quantitative and sensitive data, so it is considered suitable for evaluation of therapeutic response. Therefore, we use FDG-PET to evaluate the therapeutic response to Donepezil in patients with DAT in this study.

Recently, most neuroimaging studies have investigated therapeutic responses to AChEIs using voxel-by-voxel analysis[4,5,11,19,20]. We reported the usefulness of SPECT to evaluate treatment response to Donepezil in patients with DAT by three-dimensional stereotaxic ROI template[19]. In these analyses spatial normalization of brain images to a standard stereotactic space is performed in order to facilitate the anatomical accuracy of subsequent voxel-based analysis[5]. However, it has been pointed out that brain atrophy cannot be completely standardized on these analyses. Therefore, we used ROI analysis in this study in order to minimize the influence of variations in brain atrophy among patients.

The reason for increased glucose metabolism in the Responders remains unclear. FDG-PET can reflect functional activity[23], but can not detect sensitive changes in the cholinergic nervous system[24]. Shinotoh, et al[9] reported that Donepezil reduced AChE activity in the cerebral cortex using PET and N-(^{11}C) methylpiperidin-4-yl acetate and suggested that the effect was likely caused by improved cholinergic activity due to inhibition of AChE in the brain. The contribution of the cholinergic deficit to cognitive abnormalities is further supported by correlations between the severity of acetylcholine deficiency and the degree of cognitive impairment in DAT[25]. These findings suggested that FDG-PET indirectly shows changes in functional activity caused by improvement in cholinergic activity after Donepezil treatment.

There are some limitations to this study. First, the sample size in this study is too small and may not reflect a typical DAT population. Second, there is a problem in the method of semiquantifying regional glucose metabolism values in this ROI analysis study. In most PET studies of DAT, cerebellar metabolism has been used as a reference region because it is less involved in the progression of DAT[26-28]. However, there is a report that cerebellar glucose metabolism is significantly reduced in advanced DAT[29]. Therefore, we excluded cases over

CDR=2 to minimize this effect and we will examine this issue further using the primary visual region as a reference region, since that area is much less involved in the disease. Third is the general limitation of ROI placement. This method has problems including inadequate reproducibility of the ROI designation procedure and inadequate objectivity[19]. Fourth, we are not able to exclude the effect of stress response during the PET scan procedure. The brain metabolism in some patients might have at least partly reflected this effect rather than the effect to Donepezil treatment. Fifth, there is a problem in the way to define the therapeutic response. The definition of the response in a progressive neurodegenerative disease can be challenging. Studies designed to evaluate definition of treatment response in patients with DAT are scarce[6]. Although there were few evidences, we regarded patients who changed by more than −1 point as Responders on ADAS-J cog in this study, because even placebo patients showed some improvement within several weeks and the mean change scores of placebo groups in ADAS-J cog was about −1 point at 12 weeks[16]. We need further research to verify this definition. Further studies will be needed to investigate the effect of Donepezil on glucose metabolism in the brains of patients with DAT. Despite these limitations, the present findings suggest that FDG-PET could be useful for monitoring the response to Donepezil in patients with DAT.

Acknowledgements

This study was supported by the Medical Research Foundation for Senile Dementia of Osaka.

References

1. Rogers SL, Farlow MR, Doody RS, Mohs R, Friedhoff LT. A 24-week, double-blind, placebo-controlled trial of donepezil in patients with Alzheimer's disease. Donepezil Study Group. Neurology 1998;50:136-145.
2. Feldman H, Gauthier S, Hecker J, Vellas B, Subbiah P, Whalen E; Donepezil MSAD Study Investigators Group. A 24-week, randomized, double-blind study of donepezil in moderate to severe Alzheimer's disease. Neurology 2001;57:613-620.
3. Birks J, Harvey RJ. Donepezil for dementia due to Alzheimer's disease. Cochrane Database Syst Rev 2006; (1):CD001190.
4. Mega MS, Dinov ID, Porter V, Chow G, Reback E, Davoodi P, et al. Metabolic patterns associated with the clinical response to galantamine therapy: a fludeoxyglucose f 18 positron emission tomographic study. Arch Neurol 2005;62:721-728.
5. Stefanova E, Wall A, Almkvist O, Nilsson A, Forsberg A, Långström B, et al. Longitudinal PET evaluation of cerebral glucose metabolism in rivastigmine treated patients with mild Alzheimer's disease. J Neural Transm 2006;113:205-218.
6. Burns A, Yeates A, Akintade L, Del Valle M, Zhang RY, Schwam EM, et al. Defining treatment response to donepezil in Alzheimer's disease: responder analysis of patient-level data from randomized, placebo-controlled studies. Drugs Aging 2008;25:707-714.
7. Alexander GE, Chen K, Pietrini P, Rapoport SI, Reiman EM. Longitudinal PET Evaluation of Cerebral Metabolic Decline in Dementia: A Potential Outcome Measure in Alzheimer's Disease Treatment Studies. Am J Psychiatry 2002;159:738-745.
8. Matsuda H. Cerebral blood flow and metabolic abnormalities in Alzheimer's disease. Ann Nucl Med 2001; 15:85-92.
9. Shinotoh H, Aotsuka A, Fukushi K, Nagatsuka S, Tanaka N, Ota T, et al. Effect of donepezil on brain acetylcholinesterase activity in patients with AD measured by PET. Neurology 2001;56:408-410.
10. Nakano S, Asada T, Matsuda H, Uno M, Takasaki M. Donepezil hydrochloride preserves regional cerebral blood flow in patients with Alzheimer's disease. J Nucl Med 2001;42:1441-1445.
11. Modrego PJ. The effect of drugs for Alzheimer disease assessed by means of neuroradiological techniques. Curr Med Chem 2006;13:3417-3424.
12. Teipel SJ, Drzezga A, Bartenstein P, Moller HJ, Schwaiger M, Hampel H. Effects of donepezil on cortical metabolic response to activation during (18)FDG-PET in Alzheimer's disease: a double-blind cross-over

trial. Psychopharmacology (Berl) 2006;187:86-94.
13. Tune L, Tiseo PJ, Ieni J, Perdomo C, Pratt RD, Votaw JR, et al. Donepezil HCl (E2020) maintains functional brain activity in patients with Alzheimer disease: results of a 24-week, double-blind, placebo-controlled study. Am J Geriatr Psychiatry 2003;11:169-177.
14. American Psychiatric Association. Diagnostic and Statistical Manual of Mental Disorders. Washington DC: American Psychiatric Association, 2004.
15. Kim KW, Lee DY, Jhoo JH, Youn JC, Suh YJ, Jun YH, et al. Diagnostic accuracy of mini-mental status examination and revised hasegawa dementia scale for Alzheimer's disease. Dement Geriatr Cogn Disord 2005;19:324-330.
16. Homma A, Takeda M, Imai Y, Udaka F, Hasegawa K, Kameyama M, et al. Clinical efficacy and safety of donepezil on cognitive and global function in patients with Alzheimer's disease. A 24-week, multicenter, double-blind, placebo-controlled study in Japan. E2020 Study Group. Dement Geriatr Cogn Disord 2000;11: 299-313.
17. Mizumura S, Kumita S. Stereotactic statistical imaging analysis of the brain using the easy Z-score imaging system for sharing a normal database. Radiat Med 2006;24:545-552.
18. Mega MS, Cummings JL, O'Connor SM, Dinov ID, Reback E, Felix J, et al. Cognitive and metabolic responses to metrifonate therapy in Alzheimer disease. Neuropsychiatry Neuropsychol Behav Neurol 2001; 14:63-68.
19. Higashiyama S, Kawabe J, Hashimoto H, Akiyama H, Kawamura E, Torii K, et al. 3DSRT evaluation of responses of Alzheimer type dementia to donepezil hydrochloride therapy. Osaka City Med J 2006;52:55-62.
20. Tateno M, Kobayashi S, Utsumi K, Morii H, Fujii K. Quantitative analysis of the effects of donepezil on regional cerebral blood flow in Alzheimer's disease by using an automated program, 3DSRT. Neuroradiology 2008;50:723-727.
21. Rosen WG, Mohs RC, Davis KL. A new rating scale for Alzheimer's disease. Am J Psychiatry 1984;141: 1356-1364.
22. Mega MS, Masterman DM, O'Connor SM, Barclay TR, Cummings JL. The spectrum of behavioral responses to cholinesterase inhibitor therapy in Alzheimer disease. Arch Neurol 1999;56:1388-1393.
23. Sokoloff L. Mapping of local cerebral functional activity by measurement of local cerebral glucose utilization with [14C]deoxyglucose. Brain 1979;102:653-668.
24. Le Mestric C, Chavoix C, Chapon F, Mézenge F, Epelbaum J, Baron JC. Effects of damage to the basal forebrain on brain glucose utilization: a reevaluation using positron emission tomography in baboons with extensive unilateral excitotoxic lesion. J Cereb Blood Flow Metab 1998;18:476-490.
25. Bierer LM, Haroutunian V, Gabriel S, Knott PJ, Carlin LS, Purohit DP, et al. Neurochemical correlates of dementia severity in Alzheimer's disease: relative importance of the cholinergic deficits. J Neurochem 1995; 64:749-760.
26. Pickut BA, Dierckx RA, Dobbeleir A, Audenaert K, Van Laere K, Vervaet A, et al. Validation of the cerebellum as a reference region for SPECT quantification in patients suffering from dementia of the Alzheimer type. Psychiatry Res 1999;90:103-112.
27. Levy-Cooperman N, Burhan AM, Rafi-Tari S, Kusano M, Ramirez J, Caldwell C, et al. Frontal lobe hypoperfusion and depressive symptoms in Alzheimer disease. J Psychiatry Neurosci 2008;33:218-226.
28. Kobayashi S, Tateno M, Utsumi K, Takahashi A, Saitoh M, Morii H, et al. Quantitative analysis of brain perfusion SPECT in Alzheimer's disease using a fully automated regional cerebral blood flow quantification software, 3DSRT. J Neurol Sci 2008;264:27-33.
29. Ishii K, Sasaki M, Kitagaki H, Yamaji S, Sakamoto S, Matsuda K, et al. Reduction of cerebellar glucose metabolism in advanced Alzheimer's disease. J Nucl Med 1997;38:925-928.

Neuroimage 59 (2012) 3149–3158

Contents lists available at SciVerse ScienceDirect

NeuroImage

journal homepage: www.elsevier.com/locate/ynimg

A short-scan method for k_3 estimation with moderately reversible PET ligands: Application of irreversible model to early-phase PET data

Koichi Sato [a,b,*], Kiyoshi Fukushi [a], Hitoshi Shinotoh [a,c], Hitoshi Shimada [a], Noriko Tanaka [a,d], Shigeki Hirano [a,e], Toshiaki Irie [a]

[a] Molecular Imaging Center, National Institute of Radiological Sciences, 4-9-1 Anagawa, Inage-ku, Chiba 260-8555, Japan
[b] Department of Psychiatry, Teikyo University Chiba Medical Center, 3426-3 Anesaki, Ichihara-shi, Chiba 299-0111, Japan
[c] Asahi Hospital for Neurological Diseases and Rehabilitation, 789-10 Kurigasawa, Matsudo-shi, Chiba 270-0022, Japan
[d] Department of Neurosurgery, Tokyo Women's Medical University Medical Center East, 2-1-10 Nishiogu, Arakawa-ku, Tokyo 116-8567, Japan
[e] Department of Neurology, Graduate School of Medicine, Chiba University, 1-8-1 Inohana, Chuo-ku, Chiba 260-8677, Japan

ARTICLE INFO

Article history:
Received 21 June 2011
Revised 8 October 2011
Accepted 25 October 2011
Available online 4 November 2011

Keywords:
[^{11}C]PIB
Compartment models
Information density
PET
Reversible ligand
Tracer kinetics

ABSTRACT

Long dynamic scans (60–120 min) are often required for estimating the k_3 value, an index of receptor density, by positron emission tomography (PET). However, the precision of k_3 is usually low in kinetic analyses for reversible PET ligands compared with irreversible ligands. That is largely due to unstable estimation of the dissociation rate constant, k_4. We propose a novel '3P+' method for estimating k_3 of moderately reversible ligands, where a 3-parameter model without k_4 is applied to early-phase PET data to obtain a good model-fit of k_3 estimation. By using [^{11}C] Pittsburgh compound B (PIB) ($k_4 = 0.018$/min) as an example of a moderately reversible ligand, the 3P+ method simulation with a 28 min PET scan yielded less than 3% k_3 relative bias with a +100% k_3 change. In [^{11}C]PIB PET scans of 15 normal controls (NC) and nine patients with Alzheimer's disease (AD), the 3P+ method provided a precise k_3 estimate (mean SE of 13.6% in parietal cortex; covariance matrix method). The results revealed linear correlations ($r = 0.964$) of parietal k_3 values in 24 subjects between 28 minute 3P+ method and conventional 90 minute 4-parameter method. A good separation of k_3 between NC and AD groups ($P < 0.001$; t-test) was replicated in 28 minute 3P+ method. The short-scan 3P+ method may be a practical alternative method for analyzing reversible ligands.

Introduction

Two classes of positron emission tomography (PET) ligands, namely, reversible and irreversible (or metabolic trapping) ligands, are currently used for in vivo measurement of receptors and enzymes in the brain. However, the PET scan duration time needed for compartmental analysis and precise model-parameter estimation substantially differs between reversible and irreversible ligands.

In irreversible ligands, the tissue time–activity curve (TAC) is described with a 2-tissue compartment 3-parameter (K_1–k_3) model (3P model), not involving k_4. K_1 refers to the transport rate constant from blood to tissue, k_2 is the efflux rate constant from tissue to blood, k_3 is the rate constant for specific binding, and k_4 represents the dissociation rate constant. The k_3 represents $B_{max} \cdot k_{on}$, where B_{max} is the maximum density of receptors and k_{on} is the in vivo association rate constant, and is thus the target parameter of major interest for receptor quantification. In the 3P model, except for ligands with an extremely high k_3-to-k_2 ratio (Kilbourn et al., 1998), it is possible to estimate k_3 with greater precision than the 2-tissue compartment 4-parameter (K_1–k_4) model (4P model). Moreover, this can be achieved with a shorter dynamic PET scan (40–60 min) since there is no need for k_4 estimation from the PET measurement of the equilibrium-phase of tracer kinetics (equilibrium analysis). For example, in studies using *N*-[^{11}C]methylpiperidin-4-yl acetate ([^{11}C]MP4A) and propionate ([^{11}C]MP4P or [^{11}C]PMP), the radioactive acetylcholine analogs of the metabolic-trapping type, cerebral cortical k_3 (an index of acetylcholine esterase activity) can be estimated from a 40–60 min dynamic PET scan. The results of previous studies using regions-of-interest (ROI) analyses revealed a coefficient-of-variation (CV) of less than 15% in healthy volunteers (Namba et al., 1999; Koeppe et al., 1999; Sato et al., 2004). Statistical analysis of voxel-by-voxel k_3 in the cerebral cortex has also been conducted with [^{11}C]MP4A PET (Shimada et al., 2009).

In reversible ligands, the tissue TAC is usually described with a 4P model. In the 4P model, a long PET measurement period is typically required, extending over 60 min even with relatively fast-kinetics ligands with moderate k_4. However, the precision of k_3 estimates in

* Corresponding author at: Department of Psychiatry, Teikyo University Chiba Medical Center, 3426-3 Anesaki, Ichihara-shi, Chiba 299-0111, Japan. Fax: +81 436 62 1511.
E-mail addresses: ksatok@med.teikyo-u.ac.jp (K. Sato), fukushi@nirs.go.jp (K. Fukushi), hitoshi.shinoto@nifty.com (H. Shinotoh), shim@alpha.ocn.ne.jp (H. Shimada), tanakane@dnh.twmu.ac.jp (N. Tanaka), s_hirano@chiba-u.jp (S. Hirano), t_irie@nirs.go.jp (T. Irie).

1053-8119/$ – see front matter © 2011 Elsevier Inc. All rights reserved.
doi:10.1016/j.neuroimage.2011.10.087

the 4P model is often imprecise for receptor quantification, largely due to instability of k_4 estimation in the late phase of PET acquisition. Therefore, only few reports have investigated the direct estimation of k_3 in reversible ligands. Instead of k_3, more robust output measures in the 4P model such as binding potential (BP_{ND}; the k_3-to-k_4 ratio) and total distribution volume (DV) are widely used as practical indices of neuroreceptor function (Mintun et al., 1984; Hume et al., 1992; Innis et al., 2007; Logan et al., 1990).

In this article, we propose a novel strategy for k_3 estimation for moderately reversible PET ligands. In this method, the 3P model without k_4 is used with early-phase PET data such as 0–30 min TAC from reversible ligands. We refer to this strategy as '3P+', meaning 3P model analysis plus a short PET scan time. In describing this strategy, we introduce new concepts such as information density and TAC segmentation. Then, we assess the precision and bias of our k_3 estimate with the 3P+ method in comparison with a standard 4P analysis in a Monte-Carlo simulation, as well as in a clinical evaluation using the amyloid binding radiotracer [^{11}C]Pittsburgh compound B (PIB) as an example of a moderately reversible ligand. Although simple and practical methods for the estimation of BP_{ND} and DV have been established in [^{11}C]PIB PET (Price et al., 2005; Lopresti et al., 2005; Lammertsma et al., 1996; Lammertsma and Hume, 1996; Wu and Carson, 2002; Ichise et al., 1996; Logan et al., 1990), a comparison of the performance between the 3P+ method and previous analyses in [^{11}C]PIB PET is beyond the scope of the present study, and will be presented separately.

Theory

Information density function

In the 4P model for reversible ligands, the tissue TAC in the baseline state and in four altered states can be represented as follows:

$$\text{Baseline} = \text{TAC}(K_1, k_2, k_3, k_4, t) \tag{1}$$

$$\text{Alteration(i)} = \text{TAC}(k_i + \Delta k_i, t), i = 1, 2, 3 \text{ and } 4. \tag{2}$$

The difference between each alteration(i) TAC and the baseline TAC depends on changes in each parameter, Δk_i. The residual TAC, ΔTAC(t), is defined as the difference between the alteration(i) and the baseline TAC:

$$\begin{aligned}\Delta\text{TAC}(k_i, t) &\equiv \text{Alteration(i)} - \text{Baseline} \\ &= \text{TAC}(k_i + \Delta k_i, t) - \text{TAC}(k_i, t),\ i = 1, 2, 3 \text{ and } 4.\end{aligned} \tag{3}$$

If the sum of squared residuals, $[\Delta\text{TAC}(k_i, t_j)]^2$ (j = 1 to N, N is total frame number), is small for a given Δk_i (i.e. distance of two TAC is small), it is difficult to detect such a parameter change from the observed TAC change. That is, TAC changes are insensitive to parameter changes. In other words, TACs contain little information for estimating the parameter.

As such, we define the information density function, $ID(k_i,t)$, using $[\Delta\text{TAC}(k_i, t)]^2$ after normalization for parameter changes to +10% and conversion to a continuous function of time as follows:

$$ID(k_i, t) = \frac{[\Delta\text{TAC}(k_i, t)]^2}{\Delta k_i / k_i},\ i = 1, 2, 3 \text{ and } 4. \tag{4}$$

Fig. 1A shows an example of $ID(k_i,t)$ functions of K_1–k_4 calculated for [^{11}C]PIB up to 90 min after tracer injection. In the inset of Fig. 1A, the curves of k_3 and k_4 are shown up to 300 min. In this calculation, baseline TAC was generated using an analytic solution of the 4P model with parameter set in the [^{11}C]PIB baseline condition, namely, K_1 = 0.180 mL/g/min, k_2 = 0.180/min, k_3 = 0.018/min and k_4 = 0.018/min and input function derived from a representative normal subject in a clinical [^{11}C]PIB study. The four model-parameters revealed markedly

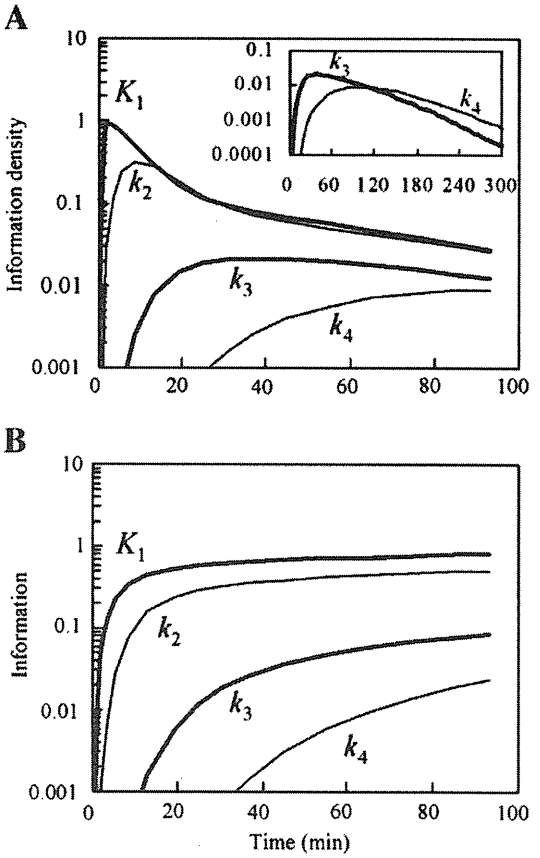

Fig. 1. Example of information density function (A) and information function (B) calculated for [^{11}C]PIB in the baseline condition: K_1 = 0.180 mL/g/min, k_2 = 0.180/min, k_3 = 0.018/min, and k_4 = 0.018/min and input function obtained from a representative normal subject. In the inset of A, the curves of k_3 and k_4 are shown up to 300 min.

different peak-times in the $ID(k_i,t)$ curves; 2.5 min for K_1, 9.3 min for k_2, 37 min for k_3, and 101 min for k_4. These results indicate that TAC information for estimation of each parameter in the 4P model is non-uniformly distributed along PET scan time and appears sequentially from K_1 to k_4; K_1 information appears in the very early-phase of the TAC, followed by k_2 and k_3, and k_4 information only occurs in the latest-phase of the TAC.

Information function

Next, we define the information function $I(k_i,t)$ as a time-integral of the $ID(k_i,t)$ function. This function represents the total amount of information included within a portion of the TAC from time = 0 to t,

$$I(k_i, t) = \int_0^t ID(k_i, \tau)d\tau,\ i = 1, 2, 3 \text{ and } 4. \tag{5}$$

Fig. 1B shows $I(k_i,t)$ curves calculated for [^{11}C]PIB as an example. The values (in relative scale) of $I(k_i,t)$ were: 3.3×10^{-3} for K_1, 8.0×10^{-6} for k_2, 1.3×10^{-10} for k_3, and 1.3×10^{-15} for k_4 at 1 min; 0.57 for K_1, 0.29 for k_2, 0.011 for k_3, and 0.00028 for k_4 at 28 min; and 0.79 for K_1, 0.49 for k_2, 0.078 for k_3, and 0.019 for k_4 at 90 min.

There is a close relationship between $I(k_i,t)$ (information of k_i) and parameter SE (precision of k_i) in a nonlinear least-squares (NLS) analysis. A parameter with large $I(k_i,t)$, such as K_1, can be estimated with small SE (high precision). Since the $I(k_4)$ curve is relatively low, indicating that k_4 information is poor, a long PET scan is required to estimate k_4

accurately. The I(k_4) curve only slowly increased, exceeding 0.001 at about 35 min (Fig. 1B). Thus, k_4 process may have little effect on the [^{11}C]PIB TAC between 0 and 35 min after tracer injection.

Theoretical basis of 3P+

To explain the 3P+ method, we further introduce two basic concepts, TAC segmentation and stepwise parameter estimation. Based on ID(k_i,t) and I(k_i,t) curves calculated for [^{11}C]PIB of above, the whole 90 min TAC can be divided into three segments (Fig. 2A); the K_1-segment (0–1 min), k_2/k_3-segment (1–28 min), and k_4-segment (28–90 min). The k_4 contribution to the TAC is thought to be negligible within the time period prior to the X-intercept of the I(k_4) curve, and similarly the k_2 contribution is negligible within the time period prior to the X-intercept of the I(k_2) curve (Fig. 1B). Therefore, two transition times (1 and 28 min) were determined in accordance with the X-intercepts (Y = 0.001) of the I(k_2) and I(k_4) curves. In the K_1-segment, the tissue TAC is dependent on only K_1, with a large amount of information about K_1. In the k_2/k_3-segment, the TAC is dependent on K_1, k_2 and k_3 but not on k_4, with a sufficient amount of information about k_2 and k_3. In the k_4-segment, the TAC is dependent on all parameters, including k_4. Within a portion of the TAC (K_1-segment or k_2/k_3-segment), a more simplified model is used for the stepwise estimation of k_i (i = 1–4). That is, for any PET tracer, the appropriateness of the model-configuration is determined by the scan time rather than by the tracer's properties. The simplified model is described as follows.

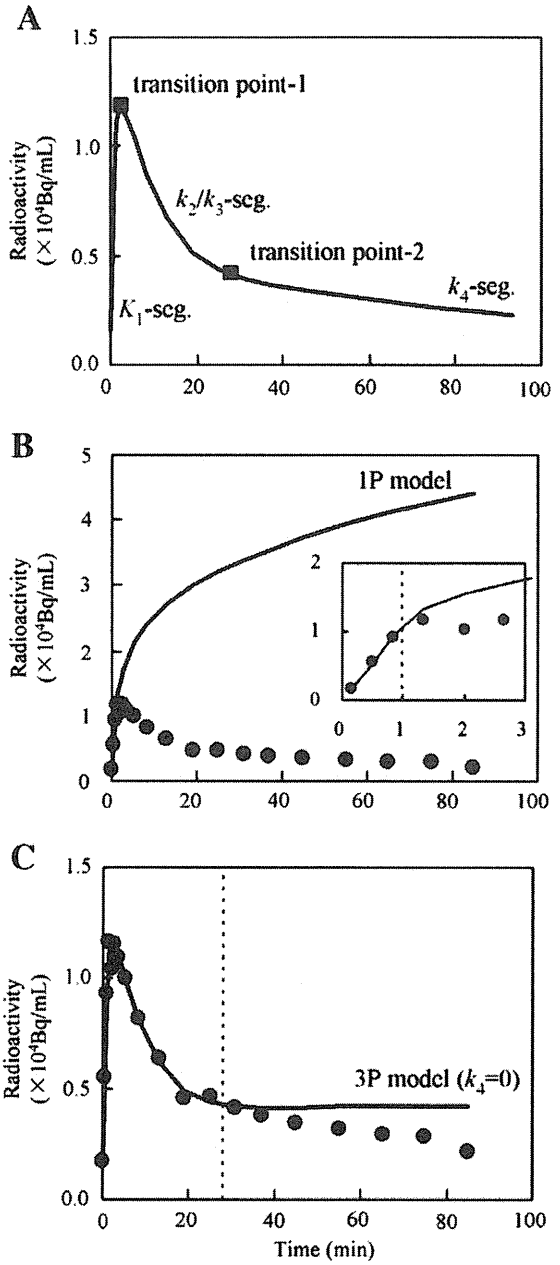

Fig. 2. Schematic representation of "TAC segmentation" with two transition points (1 and 28 min, ■) (A), and the fits of a noisy [^{11}C]PIB TAC (●) to 1P model (solid line) in K_1-segment (0–1 min) (B) and to 3P model (solid line) in K_1- and k_2/k_3-segments (0–28 min) (C). Inset graph of B corresponds to data at extremely early times (0–3 min). The dotted lines in B and C indicate the transition times (1 and 28 min).

First, blood flow measurement is considered. The target parameter is K_1. Here, we suppose that a diffusible radiotracer is administered by constant infusion for 1 min. Since washout of the tracer is negligible during the infusion period, the tracer's behavior during 0–1 min (K_1-segment) can be described by a single parameter (1P) model (microsphere model). Fig. 2B shows the fit of a noisy [^{11}C]PIB TAC to the 1P model during the infusion period (0–1 min). The 1P model shows a good fit in the extremely early-phase of TAC (K_1-segment), indicating that within the K_1-segment, the TAC of any diffusible tracer can be described with the 1P model, and that the approximate K_1 value, i.e. cerebral blood-flow, can be estimated based on the 1P model.

Next, receptor quantification using reversible PET ligands is considered. The target parameter with this method is k_3. Since the k_4 process is negligible until approximately 35 min in [^{11}C]PIB (Fig. 1B), the 3P model ($k_4 = 0$ model) may be applicable to the K_1- and k_2/k_3-segments in [^{11}C]PIB. Fig. 2C shows a curve fitted to the 3P model. Again, K_1–k_3 can be estimated from a 0–28 min TAC portion with a 3P model. This strategy for three-parameter estimation is abbreviated to '3P+', or specifically to '3P+_28min' when the PET scan time is 28 min. A standard four-parameter estimation method for reversible ligands is abbreviated here to '4P', or specifically to '4P_90min' when the PET scan time is 90 min.

Materials and methods

Monte-Carlo simulation

Noise-free TAC data (19 frames/90 min) were generated based on a 4P model using the same parameter set and input function as the [^{11}C]PIB baseline TAC described above. SD of additive noise $\sigma(C_i)$ was generated using pseudo random numbers from a Gaussian distribution with a mean of 0 and variance of 1, to simulate counting statistics based on ^{11}C, according to the following formula (Logan et al., 2001):

$$\sigma(C_i) = \varepsilon\sqrt{\frac{C_i}{\Delta t_i \cdot \exp(-\lambda t_i)}} \tag{6}$$

where C_i is noise-free simulated radioactivity concentration at frame number i, ε is a scaling factor that determines the noise level, Δt_i is scan duration of frame number i, t_i is mid-scan time of frame number i, and λ is ^{11}C decay constant. $\varepsilon = 1.6$ was used in the present simulation, as empirically determined from actual PET data; this is considered a relatively high noise level. In NLS analysis, a positivity constraint was used for all k_i. In all Monte-Carlo simulations, a data set of 100 noisy TACs was analyzed with weighted NLS, using a relative weight w_i given as:

$$w_i = \text{constant} \cdot \frac{\Delta t_i \cdot \exp(-\lambda t_i)}{C_i}. \tag{7}$$

Evaluation of goodness-of-fit

The reduced Chi-squared statistic was used as a measure of the goodness-of-fit of models under different model-configurations and/or a different number of data points, defined as follows:

$$\text{reduced}\,\chi^2 = \frac{\chi^2}{n-p-1} \tag{8}$$

where χ^2 is the weighted residual sum-of-square (i.e. Chi-squared), n is the number of independent measurements (dynamic acquisitions), and p is the number of fitted parameters in the model, i.e. $n-p-1$ refers to the degrees of freedom. In Monte-Carlo simulation, 100 simulated TACs, ranging 11 frames (22 min) to 19 frames (90 min), were analyzed using the NLS method; the reduced χ^2 was computed as the mean of the 100 values for each simulation.

Evaluation of k_3 CV

Monte-Carlo simulation was used for relative comparison of k_3 precision between 3P and 4P analyses. PET scan duration times were between 22 and 90 min in the 3P analysis, and between 60 and 90 min in the 4P analysis. A data set of 100 simulated TACs was subjected to NLS analysis, producing the mean and SD of 100 k_3 estimates. As a measure of k_3 precision, k_3 CVs were calculated as follows:

$$\text{CV}(\%) = \frac{\text{SD}}{\text{mean}} \times 100. \tag{9}$$

To examine the dependency of k_3 CV on the ligand k_4, a Monte-Carlo simulation was performed with k_4 values of 0.006, 0.018 and 0.036/min.

Evaluation of absolute and relative k_3 biases in 3P+

Error-free simulation was used to evaluate k_3 bias in the 3P+ analysis. It should be noted that because simulated TAC data were generated from the 4P model, the 4P analysis is bias-free in error-free simulation. We propose two distinct ways to evaluate k_3 bias in the 3P+ method. One type of k_3 bias is the absolute bias in a single test, while the other is the relative bias, that is, the bias of k_3 change between test-1 and test-2 in a comparative study. These two types of bias can be defined as:

$$\text{absolute bias} \equiv \frac{\text{estimated}\,k_3 - \text{true}\,k_3}{\text{true}\,k_3} \times 100(\%) \tag{10}$$

$$\text{relative bias} \equiv \frac{\text{estimated}\,k_3\text{change} - \text{true}\,k_3\text{change}}{\text{true}\,k_3\text{change}} \times 100(\%) \tag{11}$$

with

$$k_3\ \text{change (n - fold)} = \begin{cases} \dfrac{k_3^{\text{test-2}}}{k_3^{\text{test-1}}} & (k_3^{\text{test-2}} > k_3^{\text{test-1}}) \\ \dfrac{k_3^{\text{test-1}}}{k_3^{\text{test-2}}} & (k_3^{\text{test-2}} < k_3^{\text{test-1}}) \end{cases} \tag{12}$$

When absolute bias is constant between test-1 and test-2, the relative bias becomes zero, regardless of how large the absolute bias is. In our simulations examining relative bias, the magnitude of true k_3 changes in Eq. 12 was assumed to be 2-fold (i.e. a +100% increase or a −50% decrease in test-2 compared with test-1). In graphs showing the relation between relative k_3 bias (y-axis) and the ligand k_3 (x-axis), the x-axis was plotted as the test-1 k_3 multiplied by 1.41 (square root of 2), a geometric mean of test-1 k_3 and test-2 k_3 corresponding to a 2-fold k_3 change.

Effect of tissue heterogeneity on 3P+

To describe tissue heterogeneity, we have defined three kinds of ROIs with different k_3 as follows:

ROI_0 a cerebrospinal fluid (CSF)-like tissue with negligible k_3 of 0.005/min,
ROI_1 cerebral cortex in healthy controls (NC) with k_3 of 0.018/min,
ROI_2 cerebral cortex in patients with Alzheimer's disease (AD) with k_3 of 0.036/min.

K_1 (0.180 mL/g/min), k_2 (0.180/min), and k_4 (0.018/min) were the same among the three ROIs. ROI_0 was mixed to ROI_1 or ROI_2 with different fractions (0%–50%), resulting in simulated TACs, which were analyzed in 3P+_28min and 4P_90min analyses to assess the relative k_3 bias.

Effect of changing vascular pool on 3P+

To assess the effects of changing the vascular pool, the simulated brain TACs (ROI_1 with k_3 of 0.018/min and ROI_2 with k_3 of 0.036/min) were generated similarly as in the simulation of tissue heterogeneity but with different blood pools (3%–7%). The simulated brain TACs were then analyzed in 4P_90min and 3P+_28min analyses for a fixed blood pool fraction (5%), and the relative k_3 biases were calculated.

Evaluation of 3P+ using clinical [^{11}C]PIB data

Human subject

[^{11}C]PIB clinical data were obtained from ongoing patient studies, which had been approved by the Institutional Review Board of the National Institute of Radiological Sciences. The subjects included 15 NC ranging in age from 48 to 90 years (mean age 66 years), and nine AD ranging from 55 to 85 years of age (mean age 70 years). Each subject or family member gave written informed consent. Probable AD was diagnosed in accord with the criteria of the National Institute of Neurological and Communication Disorders, Alzheimer's Disease and Related Disorders Association (NINCDS-ADRDA; McKhann et al., 1984).

Radiochemical synthesis

[^{11}C]PIB was synthesized by the reaction of 2-(4′-aminophenyl)-6-hydroxy-benzothiazole and [^{11}C]methyl triflate (Mathis et al., 2003). The product had a radiochemical purity greater than 95.4%. Specific activity was in the range of 56.3–285.3 GBq/μmol at the time of injection.

PET scan protocol

PET images were acquired with a Siemens ECAT EXACT HR+ scanner (CTI PET systems, Inc., Knoxville, TN, USA) with an axial field of view of 155 mm, providing 63 contiguous 2.46-mm slices with 5.6-mm transaxial and 5.4-mm axial resolution. A 10 min transmission scan was first performed to measure tissue attenuation, then infusion of [^{11}C]PIB (about 370 MBq in 5 mL for 1 min) began. A PET scan in 3D mode was started after the arrival of tracer to the brain (approximately 30 s after the beginning of tracer infusion). The dynamic scans consisted of 19 frames (3×20 s, 3×40 s, 1×1 min, 2×3 min, 5×6 min, 5×10 min) with a total scan duration of 90 min. All data processing and image reconstruction were performed using standard Siemens software, which included scatter correction, randoms and dead time correction.

The protocol also included arterial sampling, starting 6 s (transit delay at the blood sampling site) after the beginning of PET scan to 85 min post injection (10×10 s, 1×30 s, 9×2 min, 6×10 min,

1×5 min; 27 samples). Metabolite analyses were performed using a radio-TLC method as reported previously (Namba et al., 1999), but with a different TLC-developing solvent (ethyl acetate : n-hexane = 2:1, vols). The total and metabolite-corrected plasma radioactivity data were fitted using a mono-exponential saturation function during infusion (0–1 min) and the sum of 3-exponentials after the end of infusion (1–85 min), as previously described (Namba et al., 1999).

The ROIs in the frontal, temporal, parietal, occipital, anterior cingulate and posterior cingulate cortices in both hemispheres (volume 1–5 mL) were placed manually on a summed PET image by referring to the corresponding magnetic resonance image.

NLS analysis of clinical [^{11}C]PIB data

Kinetic parameters of [^{11}C]PIB, K_1–k_3 in the 3P and K_1–k_4 in the 4P model, were estimated using a weighted NLS optimization with positivity constraint of all k_i and free delay-time (time difference between tracer injection and tracer arrival to the brain). A vascular volume term was fixed to 0.05 (Price et al., 2005). In this condition, NLS analyses of the cortical ROI data successfully converged in both the 3P and 4P models. The parameter SE in the NLS analysis was calculated using a covariance matrix method (Carson, 1986; Mazoyer et al., 1986; Nagatsuka et al., 2001). In this article, results in the parietal cortex were shown as representative of the rest of the cortex. The results were essentially the same in other brain regions.

Results

Goodness-of-fit

Fig. 3 compares the dependency of goodness-of-fit on PET scan time between the 3P and 4P models. The 4P model showed a reduced χ^2 of nearly 1.0 (a good fit) in all scan duration times examined, ranging between 22 and 90 min. The 3P model provided good fits only with relatively short scan times ranging between 22 and 40 min, and thereafter, reduced χ^2 values rapidly increased (worse fit) as scan time became longer. With short scan times (22–40 min), the 3P model showed a model-fit comparable with or even better than the 4P model, the true model in the present simulation.

Bias of k_3 estimate in 3P+

Both absolute and relative k_3 biases in the 3P+ model were evaluated in an error-free simulation using error-free TACs generated from the 4P model. Fig. 4A shows the dependency of k_3 biases on the ligand k_4.

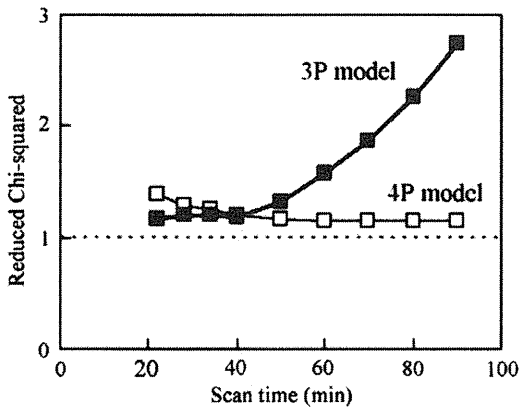

Fig. 3. Comparison of scan time dependency of goodness-of-fit (reduced Chi-squared residual) between 3P (■) and 4P (□) models. The dotted line indicates the line of reduced $\chi^2 = 1$ (best fit).

In this simulation, ligand k_3 was fixed to 0.018/min, and scan time was fixed at 28 min. Though absolute k_3 bias (negative biases) was found to be highly dependent on ligand k_4, ranging from −8.5% at k_4 = 0.006/min to −50.3% at k_4 = 0.050/min, the relative k_3 bias remained below −3.8% with a +100% k_3 change for the examined k_4 values.

Fig. 4B shows the dependency of k_3 biases in 3P+_28min on ligand k_3. In this simulation, ligand k_4 was fixed to 0.018/min. Again,

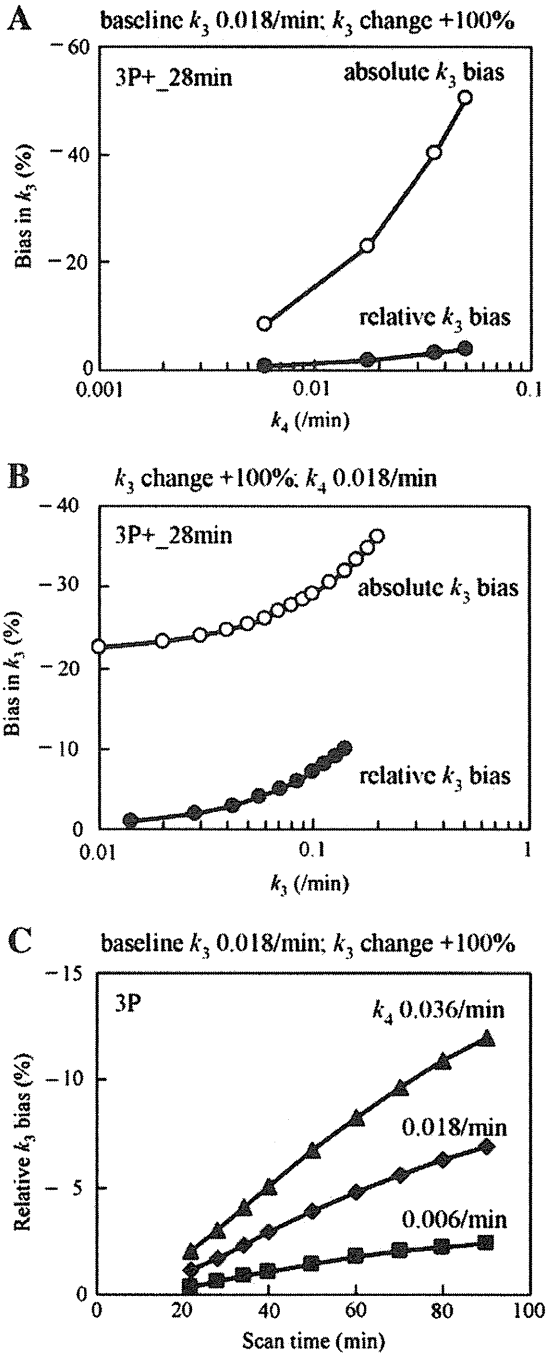

Fig. 4. (A) Dependency of absolute k_3 bias (○) and relative k_3 bias (●) in 3P+_28min analysis on ligand k_4 in the [^{11}C]PIB baseline condition except k_4. (B) Dependency on ligand k_3. The k_3 ranges were 0.010 – 0.200/min in absolute k_3 bias (○) and 0.014 – 0.141/min in relative k_3 bias (●). In the latter, k_3 values are plotted as geometric means of test-1 k_3 and test-2 k_3. (C) Comparison of scan time dependency of relative k_3 bias in 3P+ analysis among three ligands k_4 values; 0.006 (■), 0.018 (♦) and 0.036/min (▲).

the results showed that the absolute k_3 bias was high, and dependent on k_3, ranging from −22.4% at $k_3 = 0.010$/min to −36.2% at $k_3 = 0.200$/min. In contrast, the relative k_3 bias in the 3P+ model was below −10% with a +100% k_3 change when the ligand k_3 was less than 0.141/min.

Fig. 4C shows the dependency of relative k_3 bias on PET scan time for three ligand k_4 values; 0.006, 0.018 and 0.036/min. In this simulation, ligand k_3 was fixed to 0.018/min. For each k_4 examined, the relative k_3 bias gradually increased as PET scan time became longer, for example, ranging from −1.1% at 22 min to −6.9% at 90 min when $k_4 = 0.018$/min. When the PET scan time was less than 28 min, the relative k_3 biases were below −3% for all examined k_4.

Comparison of k_3 CV between 3P+ and 4P analyses

Fig. 5A shows a relative comparison of k_3 precision (k_3 CV in Monte-Carlo simulation) between 3P and 4P models as a function of PET scan time. In the 4P model, k_3 CV increased rapidly as scan time reduced. In the 3P model, k_3 CV remained almost constant between 60 and 90 min, then gradually increased as scan time became shorter. The k_3 CV in the 3P+_28min analysis was comparable with that of the 4P_90min analysis in the [^{11}C]PIB baseline condition ($k_3 = 0.018$/min, $k_4 = 0.018$/min).

Fig. 5B compares the dependency of k_3 CV on ligand k_4 between 3P+_28min and 4P_90min analyses. In this simulation, k_3 was fixed to 0.018/min. As ligand k_4 became larger, from 0.006 to 0.036/min, k_3 CV values increased in both analyses. The 4P_90min analysis showed a stronger k_4-dependecy than the 3P+_28min analysis. When k_4 was larger than 0.036/min, the 4P_90min analysis produced much larger k_3 CV values than the 3P_28min analysis (data not shown).

Effect of tissue heterogeneity on 3P+

Fig. 6 shows the effect of tissue heterogeneity on relative k_3 bias in the 3P+_28min and 4P_90min analyses. As the partial volume fraction increased from 0% to 50%, the relative k_3 bias gradually increased from −1.7% to −14.5% in the 3P+_28min analysis and from 0% to −14.9% in the 4P_90min analysis.

Effect of changing vascular pool on 3P+

Fig. 7 shows the effects of changing the true vascular pool (3%–7%) on the relative k_3 bias in 3P+_28min and 4P_90min analyses. In both analyses, the vascular pool fraction (in the calculation) was fixed to 5%. In spite of a large difference in PET scan time, the two analyses showed similar vascular effects. The relative biases in 4P_90min and 3P_28min analyses were 6.0% and 6.4%, respectively, at 3% of the true vascular volume fraction, and −5.2% and −7.7%, respectively, at 7% of the vascular volume fraction.

Evaluation of 3P+ using clinical [^{11}C]PIB data

For assessment of the absolute k_3 precision, we calculated parameter SE in an NLS analysis of [^{11}C]PIB clinical data (15 NC and nine AD subjects). An example of a representative result in parietal cortex is shown in Table 1. In the 4P_90min analysis, parameter SE increased in the order of $K_1 < k_2 < k_3 <= k_4$. In the 3P+_28min analysis, the order and magnitude of k_i SE (i = 1 to 3) were relatively similar to those in the 4P_90min analysis. In the 3P+ analysis, k_3 SE decreased (k_3 precision increased) as scan time became longer, from 13.6% at 28 min to 9.6% at 40 min.

Fig. 8 shows the result of a correlation analysis of k_3 estimates between the 3P+_28min and 4P_90min analyses. A statistically significant linear correlation was observed with a regression line and correlation coefficient of $Y = 0.686X + 0.003$ ($r = 0.964$), where Y = 3P k_3 and X = 4P k_3. When the correlation was studied separately for NC and AD groups, the regression lines were $Y = 0.599X + 0.005$ ($r = 0.841$) for the NC group and $Y = 0.768X - 0.000$ ($r = 0.897$) for the AD group; these lines were visually almost identical to the line for all subjects (not shown in Fig. 8). In the 4P_90min analysis, k_3 in the NC group ranged from 0.008 to 0.025/min, and from 0.026 to 0.060/min in the

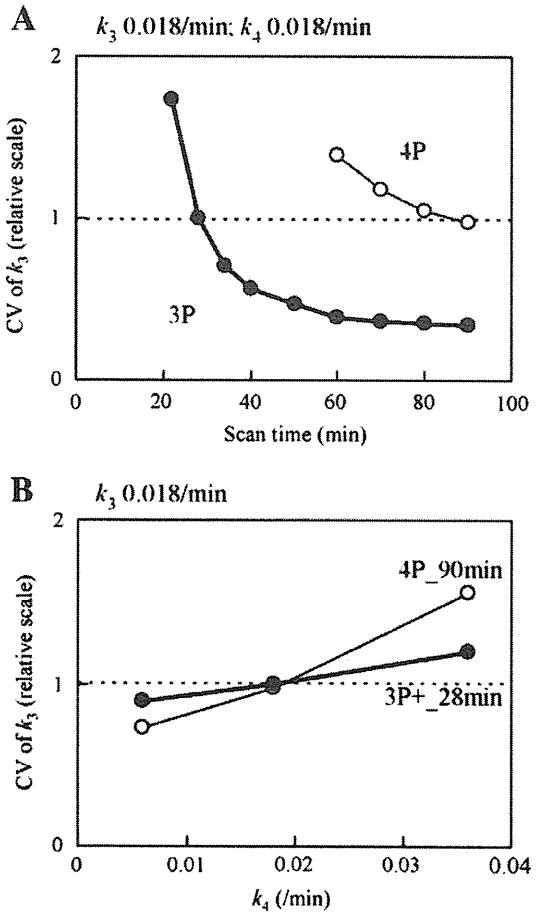

Fig. 5. (A) Relative comparison of k_3 CV in Monte-Carlo simulation between 3P model (●) and 4P model (○) as a function of PET scan time in the [^{11}C]PIB baseline condition. The k_3 CV values are shown by relative scale (k_3 CV in 3P+_28min = 1). (B) Dependency on k_3 CV on ligand k_4.

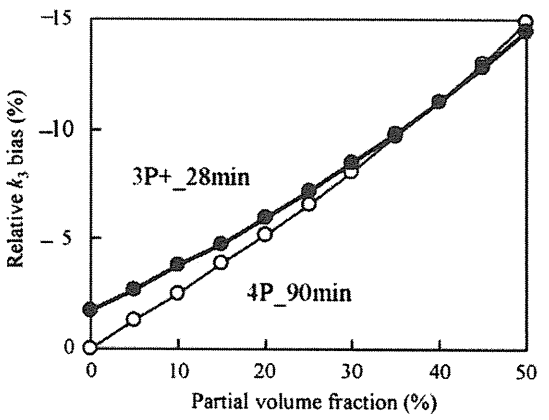

Fig. 6. Effect of tissue heterogeneity on relative k_3 bias in 3P+_28min (●) and 4P_90min (○) analyses. Tissue heterogeneity is expressed as the partial volume fraction (%), ranging from 0% to 50%, of ROI_0 (CSF; $k_3 = 0.005$/min) within either ROI_1 (NC-cortex; $k_3 = 0.018$/min) or ROI_2 (AD-cortex; $k_3 = 0.036$/min).

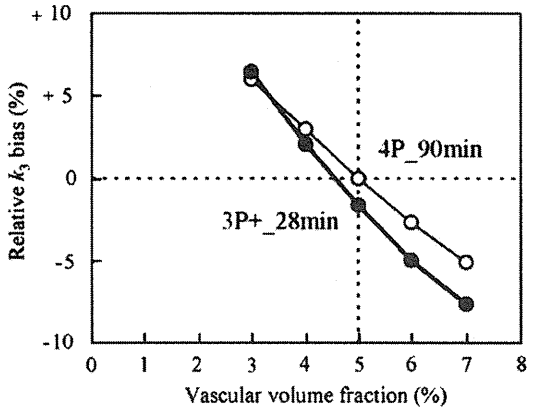

Fig. 7. Effect of the vascular volume fraction on relative k_3 bias in 3P+_28min (●) and 4P_90min (○) analyses. Simulated brain TACs were generated from [^{11}C]PIB baseline brain TACs mixed with blood TACs (3%–7%). The k_3 values of mixed TACs were estimated by fixing the vascular volume to 5%.

AD group. In 3P+_28min, k_3 in the NC group ranged from 0.009 to 0.022/min and from 0.018 to 0.047/min in the AD group. There was a significant difference in mean k_3 between the NC and AD groups ($P<0.001$; t-test). The results indicated that the NC and AD subjects were clearly separated from each other, with the exception of one AD subject, who showed results similar to the NC group.

Discussion

Theoretical basis of 3P+

The 3P+ method can be characterized in two ways. First, the method could be termed an "irreversible-model approximation", or more concisely, an "irreversible analysis". Second, it could be described as a "principle of parsimony", referring to the goal of the analysis being k_3 estimation while k_4 estimation is intentionally abandoned. In the 3P+ analysis, early-phase TAC data, referred to as K_1- and k_2/k_3-segments (0–28 min portion of TAC in [^{11}C]PIB), are fitted to an irreversible model (the 3P model). In previous studies of reversible ligands with small k_4 such as [^{18}F]fluorodeoxyglucose (Sokoloff et al., 1977) and [^{11}C]N-methylspiperone (Wong et al., 1986), k_4 has often been fixed to zero ($k_4=0$ constraint analysis). Dynamic radioligand PET data may exhibit irreversible characteristics when the time scale of the experiment is too short to fully characterize the (slow) reversible binding of the radioligand (Gunn et al., 2001). Recently, the analyses of irreversible binding ($k_4=0$ constraint analyses) of [^{11}C]PIB were also reported (Blomquist et al., 2008; Edison et al., 2009). Blomquist et al. described that PIB was far from being in equilibrium in the time interval 0–60 min; therefore, irreversible model was applied on 0–60 min TAC data in their report. Here, we proposed the 3P+ analysis with modification of '$k_4=0$ constraint analysis', where its theoretical basis, the time-range of the TAC data used for analysis, and the applicable magnitude of the k_4 of the ligands, were considered. As a result, scan time in [^{11}C]PIB PET can be reduced to 28 min compared to 60 min in the previous reports.

In a standard NLS analysis, we can calculate the variance of the parameter estimate using a covariance matrix method. The magnitude of the variance in the 4P analysis is usually in the increasing order of $K_1<k_2<k_3<=k_4$, as in the 4P_90min analysis of [^{11}C]PIB kinetics (Table 1). This implies that tissue TAC contains different amounts of information for each parameter K_1–k_4 in a given total PET scan time, and that the amount of k_4 information is the lowest among the four parameters. This notion is in accord with a more quantitative explanation based on two newly defined functions, ID(k_i,t) and I(k_i,t) functions.

Compared with the ID(k_i) curves of K_1–k_3, the ID(k_4) curve exhibited the lowest peak around 100 min in the [^{11}C]PIB baseline condition (Fig. 1A), explaining why a long dynamic PET scan extending over 60 min is required to estimate k_4 in the 4P model. The I(k_i) function represents the total amount information within a TAC. Again, the I(k_4) curve was the lowest among the four parameters (Fig. 1B), indicating that k_4 information was very poor. The k_4 information began to appear in TACs around 40 min after tracer injection, suggesting that the effect of k_4 process may be negligible in early-phase TAC.

A long PET measurement period reaching near equilibrium state is required for k_3 estimation in the 4P model, because the k_4 information in TAC is low and the correlation between k_3 and k_4 estimates in NLS analysis is high. If ^{11}C decay was taken into account, the I(k_4) curve would become much lower than in a decay-corrected calculation. In the 3P+ model, only early-phase TAC (i.e. K_1- and k_2/k_3-segments) is required for k_3 estimation, where TACs are almost independent of k_4. The 3P+ model is based on previous findings with [^{11}C]MP4A (Namba et al., 1999) and [^{11}C]MP4P (or [^{11}C]PMP) (Koeppe et al., 1999; Sato et al., 2004) showing that a short PET scan period is sufficient for precise k_3 estimation in irreversible ligands with an adequate k_3-to-k_2 ratio in the target tissue.

Goodness-of-fit in 3P+

In the present study, the 4P model was used to generate brain TAC data for simulation. Thus, it is a natural consequence that the reduced χ^2 values of the 4P model were close to 1.0 (the best fit) for all scan time conditions examined (Fig. 3). In the 3P model, good fits were obtained only in short PET scans (22–40 min) (Fig. 3), where the k_4 process had a negligible effect on TAC as predicted from I(k_4) curve (Fig. 1B). In the 3P+ analyses, long PET scans extending over 60 min are redundant, because of poor model-fit. These results were in agreement with a

Table 1
Comparison of parameter SE between 3P+ and 4P analyses using [^{11}C]PIB PET clinical data and a covariance matrix method (NC = 15, AD = 9; parietal cortex).

Analysis	Group	Parameter SE (%)			
		K_1	k_2	k_3	k_4
4P_90min	Total	2.2	4.7	13.2	14.2
	NC	1.8	3.3	11.5	13.2
	AD	2.7	6.8	15.7	15.8
3P+_28min	Total	2.2	5.1	13.6	–
	NC	2.3	4.2	13.4	–
	AD	2.6	6.6	14.0	–
3P+_34min	Total	2.3	4.4	10.6	–
	NC	2.2	3.5	10.3	–
	AD	2.5	5.6	11.0	–
3P+_40min	Total	2.2	4.0	9.6	–
	NC	2.1	3.3	9.3	–
	AD	2.4	5.1	10.0	–

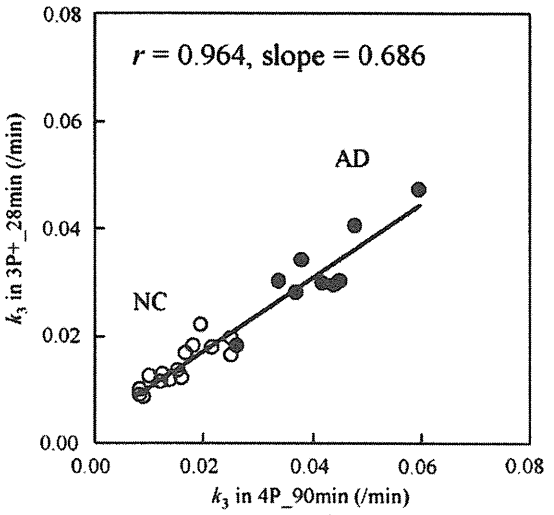

Fig. 8. Correlation of parietal-cortex k_3 estimates in 24 subjects (NC = 15, ○; AD = 9, ●) between 3P+_28min and 4P_90min analyses. The regression line and correlation coefficient are Y = 0.686X + 0.003 (r = 0.964).

previous report (Blomquist et al., 2008) which described poor fits with the 3P+ model in the time interval 0–60 min in [^{11}C]PIB PET.

Bias in 3P+: significance of relative k_3 bias rather than absolute k_3 bias in PET application

In many applications of in vivo receptor studies using PET, relative comparisons of PET results are of most concern (e.g. comparisons between patients and normal controls, regional comparisons within a single subject, and PET evaluation of efficacy between two therapeutics). In these cases, relative k_3 bias (Eqs. 11 and 12) is considered to be of more importance than the absolute bias (Eq. 10). However, most previous studies have only evaluated the absolute bias.

Because of the irreversible-model ($k_4 = 0$) approximation, the 3P+ model gives a k_3 estimate that is smaller than the true k_3. That is, roughly speaking, 3P k_3 = 4P k_3 − 4P k_4. In the 3P+ model, the larger the ligand k_4, the larger the absolute k_3 bias (negative bias). In error-free simulation, the absolute k_3 bias in the 3P+ analysis was highly dependent on the ligand k_4 value, which was more than −20% in [^{11}C]PIB with k_4 of 0.018/min (Fig. 4A). However, the relative k_3 bias was much lower than the absolute bias. Since relative k_3 bias will be slightly larger for larger k_4 (Fig. 4A), the 3P+ method works best when k_4 has not been changed in comparative studies.

The absolute k_3 bias in the 3P+ model was also dependent on ligand k_3, with increasing bias as k_3 became large (Fig. 4B). The relative k_3 bias is expected to increase as k_3 change becomes large. However, the k_3 effect on relative k_3 bias was minimal, as long as k_3 change was not so large (e.g. within a 2-fold change). Relative k_3 bias in the 3P+ model would be acceptable (less than 3%) in [^{11}C]PIB with k_4 of 0.018/min, especially when the PET scan time was less than 40 min (Fig. 4C). In a clinical [^{11}C]PIB study, an almost 2-fold k_3 increase was observed for the AD group relative to the NC group (Fig. 8). In the simulation, therefore, a relatively large k_3 change (+100%) was considered. When the k_3 change was relatively small (+25%), the relative k_3 bias significantly decreased to <1.5% under the same condition as in Fig. 4B except for the k_3 change (data not shown).

Limitations of 3P+: k_4 constancy

Strictly speaking, the 3P+ method is inadequate for estimating k_3 by itself given the large absolute bias and our method is of interest only: a) in a clinical comparison (normal vs. patient) if k_4 is assumed to be the same for the two groups and b) in a pre vs. post comparison if k_4 is assumed to be constant in the two scans.

In 3P+ analysis, the absolute k_3 bias was very large and somewhat dependent on the ligand's k_4. Therefore, if k_4 differs between the two populations to be compared, the large absolute k_3 bias produces a significant relative k_3 bias. An appropriate validation study on "k_4 constancy" is needed before the 3P+ method is applied to comparative studies or other ligands with different kinetics, for which the assumption of k_4 constancy has not yet been validated.

In our clinical [^{11}C]PIB study, 4P_90min analysis was employed to examine the k_4 constancy between NC and AD groups. Mean cortical k_4 and SD values were 0.018 ± 0.002/min for the NC group and 0.022 ± 0.003/min for the AD group, indicating that the assumption of k_4 constancy is nearly satisfied in [^{11}C]PIB. In the cases of other ligands, because of instability in the k_4 estimation in NLS analysis with the 4P model, it is uncertain whether k_4 is constant. Nevertheless, we consider that the assumption of k_4 constancy may also be satisfied for other ligands for the two following reasons. First, most PET ligands are designed to have sufficient specificity to a single receptor. If the receptor is the same for healthy and disease groups, the assumption of k_4 constancy is satisfied. Second, output parameters (BP_{ND} and DV) in conventional analyses are useful as indices of receptor density only if k_4 is constant. Many examples of the clinical usefulness of BP_{ND} and DV suggest that k_4 is constant for other ligands.

Precision of k_3 estimate in 3P+

In the Monte-Carlo simulation without the inclusion of actual noise, only a relative comparison of k_3 precision between 3P+ and 4P analyses was possible. The Monte-Carlo simulation showed that k_3 CV in the 3P+_28min analysis was comparable or slightly superior to that in the 4P_90min model, with k_4 values ranging from 0.006 to 0.036/min (Fig. 5B). A reduction in scan time (70% reduction in this simulation study) should cause information loss. Based on the calculated I(k_3) values for [^{11}C]PIB, 0.011 in a 28-min scan and 0.078 in a 90-min scan (Fig. 1B), information loss is roughly estimated at about 86% (1–0.011/0.078) without taking the ^{11}C decay into account. When this decay was considered, decay-uncorrected I(k_3) values were calculated as 0.0034 in a 28-min scan and 0.0066 in a 90-min scan, corresponding to an information loss of approximately 50% (1–0.0034/0.0066). Without the reduction of the number of fitted parameters from four to three, such information loss would be expected to worsen k_3 CV in the 3P_28min analysis. However, the results of our simulation (Fig. 5A) indicated that this information loss was compensated for by the parameter reduction effect.

Optimal PET scan time in 3P+

In the 3P+ analysis, due to the $k_4 = 0$ assumption, a good model-fit was obtained only in the early-phase of the PET scan. As scan time became longer (e.g. exceeding 40 min in [^{11}C]PIB), the model-fit of the 3P+ analysis became worse which resulted in an increased k_3 bias (Fig. 4C). If the scan time is too short in [^{11}C]PIB (i.e. less than 20 min) the k_3 bias in the 3P+ method would be expected to be low. However, the precision of the k_3 estimate would be insufficient, due to information loss. Thus, optimization of PET scan time is important in the 3P+ model, by determining the optimal trade-off between bias and precision in simulations. In the [^{11}C]PIB baseline condition, three scan time conditions, i.e. 28, 34 and 40 min (in our protocol), were almost equally useful for the 3P+ method. We have chosen 28 min for the patient's convenience.

Effect of tissue heterogeneity on 3P+

It is well known from earlier FDG studies that k_4 (precisely, "apparent k_4") is sensitive to tissue heterogeneity (Schmidt et al., 1992). It has,

for example, been demonstrated that a mixture of tissues with different k_3 but both with $k_4 = 0$ results in a tissue TAC that has a finite k_4. In receptor studies, an error in k_4 due to tissue heterogeneity will be compensated by a corresponding error in k_3, such that BP_{ND} is minimally affected. It is therefore essential that effects of tissue heterogeneity when employing the proposed method are investigated. In the simulation, the relative k_3 bias was below 10% when the partial volume fraction was below 35% (Fig. 6). The tissue-heterogeneity effect in 3P+ 28min analysis was slightly larger than or comparable to that in 4P_90min analysis. As long as k_4 (precisely, "biologically true k_4") is constant between two groups in comparative studies, the effects of tissue heterogeneity on the relative k_3 bias in the 3P+ analysis are considered to be small.

Effect of changing vascular pool on 3P+

The vascular pool fraction is usually fixed to 4% or 5% in most PET studies (e.g. 5% in [^{11}C]PIB; Price et al., 2005) and it was fixed to 5% in this study. The true vascular volume is thought to vary from region to region and from patient to patient. Fixing the vascular pool fraction to a false value will introduce errors in all other parameters fitted, and these errors may increase for shorter scan durations. Therefore, the effect of vascular pool fraction on 3P+ analysis was investigated. In the simulation, a 4% (absolute) change in vascular volume fraction resulted in 14% and 11% changes in relative k_3 bias in 3P+_28min and 4P_90min analyses, respectively (Fig. 7). The vascular pool effect was slightly larger in the 3P+_28min analysis than in the 4P_90min analysis, especially when the vascular volume fraction was larger than 5%. The cerebral vascular volume of most PET ligands is usually 4%–5%. In this case, the relative k_3 bias in the 3P+_28min analysis is expected to be small—less than 2%.

Evaluation of 3P+ using clinical [^{11}C]PIB data

In our simulation, all model parameters except the parameter examined (e.g. k_3 or k_4) were fixed to specific values in the true TAC generation. There was no error in the plasma input function data. In curve fitting using the NLS method, appropriate start values were given for the fitted parameters (i.e. within narrow ranges around the true values). In addition, simulated tissue TAC data were free of motion artifacts. Thus, we evaluated the feasibility of the 3P+ analysis using clinical PET data with [^{11}C]PIB as an example of a moderately reversible ligand.

One advantage of clinical evaluation over simulation is the capability of evaluating the absolute precision of parameter estimates (i.e. parameter SE) based on the results of curve-fitting of actual ROI data. In parietal cortical ROIs from 24 subjects, the order of parameter SE was $K_1 < k_2 < k_3 <= k_4$ in the 4P_90min analysis, which was in accord with the order of $I(k_i, 90\ \text{min})$, $K_1 > k_2 > k_3 > k_4$, since parameter SE and $I(k_i)$ exhibit an inverse relationship. In the 3P+ analysis, k_3 SE values decreased (k_3 precision increased) as scan time increased, from 13.6% at 28 min to 9.6% at 40 min (Table 1), due to information gain. A Monte-Carlo simulation also showed a similar information-gain effect, that is, an improvement of k_3 precision in 3P+ method by extending the scan time from 28 min to 40 min (Fig. 5A).

Clinical evaluation indicated that k_3 SE in the 3P+_28min analysis (13.6%; Table 1) was comparable to that in the 4P_90min analysis (13.2%), in spite of a 70% reduction in scan time and 86% reduction in k_3 information. The Monte-Carlo simulation also showed a comparable k_3 CV between the 3P+_28min and 4P_90min analyses (Fig. 5A). These results support our hypothesis that the reduction in the number of fitted parameters could compensate the information loss by scan time reduction, which is needed for obtaining a reasonable model-fit. A previous study of the 4P model in [^{11}C]PIB reported a k_3 SE (11.0% in the posterior cingulate gyrus in one subject; Price et al., 2005) that was comparable to the present findings.

In the correlation analysis (Fig. 8), a strong correlation of the k_3 estimates between the 3P+_28min and 4P_90min analyses was obtained for a k_3 range of 0.01–0.06/min in 4P_90min. The slope (0.686) of the regression line indicated the absolute k_3 bias of −31.4% with the 3P+ method, which corresponded well to the absolute k_3 bias in our simulation (approximately −25% for [^{11}C]PIB k_3 range; Fig. 4B). The AD group showed higher mean k_3 than the NC group ($P<0.001$; t-test), with no overlap with the NC group (except for one AD subject), in the both the 3P+_28min and 4P_90min analyses (Fig. 8), despite the small number of AD subjects. The results obtained by 4P_90min analysis were in accord with previous results (Price et al., 2005).

In this study, the vascular volume fraction was fixed to 0.05 according to the plasma radioactivity. The ratio of plasma to whole blood radioactivity concentration was assumed to be 1. Recently, Edison et al. (2009) reported the time dependency of this ratio, where the ratio quickly rose to reach a plateau of about 1.45 at around 20 min, due to the accumulation of radiolabelled metabolites in the plasma fraction. Therefore, the vascular volume correction was also examined in one AD subject, using whole blood radioactivity (calculated from the measured plasma radioactivity and reported plasma/blood ratio as a function of time). Absolute k_3 biases in mean cortical k_3 (k_3 obtained from plasma-based vascular volume correction relative to k_3 obtained from blood-based correction) were −5.5% in 4P_90min analysis and −4.7% in 3P+_28min analysis, which were essentially equal despite the significant scan time difference.

Applicability of 3P+ to other ligands: moderate k_4

In this study, most simulations were performed under a [^{11}C]PIB baseline condition, with k_2 of 0.180/min, k_3 of 0.018/min, and k_4 of 0.018/min. In general, the 3P+ method may not be applicable to reversible PET ligands with extremely high k_3 or k_4 values. Ligands with small k_4 values (ideally $k_4 = 0$) are more suitable to the 3P+ analysis than those with large k_4 values. This technique could be generalized to reversible ligands with k_4 values of less than 0.036/min (Fig. 4C). Such a k_4 value is referred to as a "moderate k_4 value" in this study. When k_4 is larger than 0.036/min, the fit to the 3P model clearly worsens in the time interval 0–28 min owing to a larger k_4 contribution in the earlier TAC. Therefore, PET scan times of less than 28 min are required for a good model fit and small k_3 bias (relative bias). However, the 3P+ method may be inadequate in this case owing to information loss (i.e. increased k_3 CV).

For any moderately reversible ligand, the suitable scan time can be predicted from the $ID(k_4)$ and $I(k_4)$ curves as follows. First, the K_1–k_4 values for any ligand are estimated in 4P analysis. Next, using four estimated parameters, the $ID(k_i)$ and $I(k_i)$ functions are calculated. The X-intercept of the $I(k_4)$ curve then corresponds to the adequate scan time, because the k_4 contribution is negligible in the time interval from zero to the X-intercept of $I(k_4)$.

As for the ligand k_3 condition in irreversible ligands, the selection of a ligand with a proper k_3/k_2 ratio is important for precise k_3 quantification (Irie et al., 1994; Kilbourn et al., 1998; Logan, 2000). Although there is currently no consensus about the optimal k_3/k_2 ratio, ranging from 0.1 in studies with [^{11}C]MP4P ([^{11}C]PMP) (Koeppe et al., 1999) to 0.5 in studies with [^{11}C]MP4A (Namba et al., 1999), the k_3/k_2 ratio of [^{11}C]PIB was nearly optimal in the present study, ranging from approximately 0.1 in NC subjects to 0.2–0.3 in AD subjects.

Merits of 3P+

The 3P+ method has two merits over previous analyses. One is the short PET scan time involved, and the other is the capability of k_3 quantification. In clinical [^{11}C]PIB studies, two problems associated with long PET scans emerged, especially after 60 min postinjection. One problem was the input-function measurement. The other problem was the presence of motion artifacts in AD subjects. Since PET scan time

is very short in the 3P+ method (such as 28 min in [^{11}C]PIB), it can avoid these problems and may function better in practical PET studies than in simulations.

In basic research, the short scan time involved in the 3P+ method may be useful for studying rapid processes with an event duration time of 20–30 min, such as dopamine release in synapses after the administration of amphetamine. Since synaptic dopamine concentration dynamically changes with time, k_3 (the available receptors for PET ligands) also changes with time. This constitutes a non-equilibrium state of k_3. The timing between amphetamine injection and PET measurement is important for the sensitive detection of such phenomena (Morris and Yoder, 2007). In such a case, the 3P+ method with a short scan time may be more sensitive compared with equilibrium analysis (such as a Logan plot) which requires longer scan times.

Another merit of the 3P+ method is the capability of isolating k_3. Agonist-mediated internalization of receptors has been observed for a variety of neuronal receptors (Laruelle, 2000; Ginovart, 2005). Agonist-type PET ligands may not only bind and stimulate receptors, but also shift from cell surface to intracellular components, resulting in partial irreversible characteristics with subsequent trapping. Such a process may affect k_4 but not k_3. Since the 3P+ method does not involve k_4, it may be useful in quantifying k_3 in such a k_4-changing, non-equilibrium system.

Conclusions

Based on theoretical consideration of TAC information in PET, we developed a novel strategy, the '3P+' method, for estimating k_3 of moderately reversible PET ligands. In the 3P+ method, an irreversible-ligand model ($k_4 = 0$ model) is applied to early-phase PET data (i.e. 0–30 min TAC) to obtain a good model-fit. In evaluations using [^{11}C]PIB as an example of a moderately reversible ligand, the 3P+ method provided k_3 estimates with less than 3% relative bias with a +100% k_3 change, and acceptable precision (k_3 SE = 13.6%). These results indicate that information loss due to scan time reduction from 90 min in a standard 4P analysis to 28 min in the 3P+ analysis was fully compensated for by irreversible-model approximation. Since the 3P+ method is capable of k_3 quantification with short PET scans, it may be useful for kinetic analysis of relatively rapidly-changing, non-equilibrium receptor systems.

Acknowledgments

The authors thank the production team staff for the production of isotopes and the PET operation staff for the acquisition of PET images.

References

Blomquist, G., Englar, H., Nordberg, A., Ringheim, A., Wall, A., Forsberg, A., Estrada, M., Franberg, P., Antoni, G., Langstrom, B., 2008. Unidirectional influx and net accumulation of PIB. Open Neuroimaging J. 2, 114–125.

Carson, R.E., 1986. Parameter estimation on PET. In: Phelps, M.E., Mazziotta, J.C., Schelbert, H.R. (Eds.), Positron Emission Tomography and Autoradiography: Principle and Application for the Brain and Heart. Raven Press, New York, NY, pp. 347–390.

Edison, P., Brooks, D.J., Turkheimer, F.E., Archer, H.A., Hinz, R., 2009. Strategies for the generation of parametric images of [^{11}C]PIB with plasma input functions considering discriminations and reproducibility. NeuroImage 48, 329–338.

Ginovart, N., 2005. Imaging the dopamine system with in vivo [^{11}C]raclopride displacement studies: understanding the true mechanism. Mol. Imaging Biol. 7, 45–52.

Gunn, R.N., Gunn, S.R., Cunningham, V.J., 2001. Positron emission tomography compartmental models. J. Cereb. Blood Flow Metab. 21, 635–652.

Hume, S.P., Myers, R., Bloomfield, P.M., Opacka-Juffry, J., Cremer, J.E., Ahier, R.G., Luthra, S.K., Brooks, D.J., Lammertsma, A.A., 1992. Quantification of carbon-11-labeled raclopride in rat striatum using positron emission tomography. Synapse 12, 47–54.

Ichise, M., Ballinger, J.R., Golan, H., Vines, D., Luong, A., Tsai, S., Kung, H.F., 1996. Noninvasive quantification of dopamine D2 receptors with iodine-123-IBF SPECT. J. Nucl. Med. 37, 513–520.

Innis, R.B., Cunningham, V.J., Delforge, J., Fujita, M., Gjedde, A., Gunn, R.N., Holden, J., Houle, S., Huang, S.C., Ichise, M., Iida, H., Ito, H., Kimura, Y., Koeppe, R.A., Knudsen, G.M., Knuuti, J., Lammertsma, A.A., Laruelle, M., Logan, J., Maguire, R.P., Mintun, M.A., Morris, E.D., Parsey, R., Price, J.C., Slifstein, M., Sossi, V., Suhara, T., Votaw, J.R., Wong, D.F., Carson, R.E., 2007. Consensus nomenclature for *in vivo* imaging of reversibly binding radioligands. J. Cereb. Blood Flow Metab. 27, 1533–1539.

Irie, T., Fukushi, K., Akimoto, Y., Tamagami, H., Nozaki, T., 1994. Design and evaluation of radioactive acetylcholine analogs for mapping brain acetylcholinesterase (AchE) in vivo. Nucl. Med. Biol. 21, 801–808.

Kilbourn, M.R., Nguyen, T.B., Snyder, S.E., Koeppe, R.A., 1998. One for all, or one for each? Matching radiotracers and regional brain pharmacokinetics. In: Carson, R.E., Daube-Witherspoon, M.E., Herscovitch, P. (Eds.), Quantitative Functional Brain Imaging with Positron Emission Tomography. Academic Press, San Diego, CA, pp. 261–265 (BRAINPET97, proceedings).

Koeppe, R.A., Frey, K.A., Snyder, S.E., Meyer, P., Kilbourn, M.R., Kuhl, D.E., 1999. Kinetic modeling of N-[^{11}C]methylpiperidin-4-yl propionate: alternatives for analysis of an irreversible positron emission tomography tracer for measurement of acetylcholinesterase activity in human brain. J. Cereb. Blood Flow Metab. 19, 1150–1163.

Lammertsma, A.A., Hume, S.P., 1996. Simplified reference tissue model for PET receptor studies. NeuroImage 4, 153–158.

Lammertsma, A.A., Bench, C.J., Hume, S.P., Osman, S., Gunn, K., Brooks, D.J., Frackowiak, R.S.J., 1996. Comparison of methods for analysis of clinical [^{11}C]raclopride studies. J. Cereb. Blood Flow Metab. 16, 42–52.

Laruelle, M., 2000. Imaging synaptic neurotransmission with in vivo binding competition techniques: a critical review. J. Cereb. Blood Flow Metab. 20, 423–451.

Logan, J., 2000. Graphical analysis of PET data applied to reversible and irreversible tracers. Nucl. Med. Biol. 27, 661–670.

Logan, J., Fowler, J.S., Volkow, N.D., Wolf, A.P., Dewey, S.L., Schlyer, D.J., MacGregor, R.R., Hitzemann, R., Bendriem, B., Gatley, S.F., Christman, D.R., 1990. Graphical analysis of reversible radioligand binding from time-activity measurements applied to [N-^{11}C-methyl]-(−)-cocaine PET studies in human subjects. J. Cereb. Blood Flow Metab. 10, 740–747.

Logan, J., Fowler, J.S., Volkow, N.D., Ding, Y.S., Wang, G.J., Alexoff, D.L., 2001. A strategy for removing the bias in the graphical analysis method. J. Cereb. Blood Flow Metab. 21, 307–320.

Lopresti, B.J., Klunk, W.E., Mathis, C.A., Hoge, J.A., Ziolko, S.K., Lu, X., Meltzer, C.C., Schimmel, K., Tsopelas, N.D., DeKosky, S.T., Price, J.C., 2005. Simplified quantification of Pittsburgh Compound B amyloid imaging PET studies: a comparative analysis. J. Nucl. Med. 46, 1959–1972.

Mathis, C.A., Wang, Y., Holt, D.P., Huang, G.-F., Debnath, M.L., 2003. Synthesis and evaluation of ^{11}C-labeled 6-substituted 2-aryl benzothiazoles as amyloid imaging agents. J. Med. Chem. 46, 2740–2754.

Mazoyer, B.M., Huesman, R.H., Budinger, T.F., Knittel, B.L., 1986. Dynamic PET data analysis. J. Comput. Assist. Tomogr. 10, 645–653.

McKhann, G., Drachman, D., Folstein, M., Katzman, R., Price, D., Stadlan, E.M., 1984. Clinical diagnosis of Alzheimer's disease: report of the NINCDS-ADRDA Work Group under the auspices of Department of Health and Human Services Task Force on Alzheimer's Disease. Neurology 34, 939–944.

Mintun, M.A., Raichle, M.E., Kilbourn, M.R., Wooten, G.F., Welch, M.J., 1984. A quantitative model for the in vivo assessment of drug binding sites with positron emission tomography. Ann. Neurol. 15, 217–227.

Morris, E.D., Yoder, K.K., 2007. Positron emission tomography displacement sensitivity: predicting binding potential change for positron emission tomography tracers based on their kinetic characteristics. J. Cereb. Blood Flow Metab. 27, 606–617.

Nagatsuka, S., Fukushi, K., Shinotoh, H., Namba, H., Iyo, M., Tanaka, N., Aotsuka, A., Ota, T., Tanada, S., Irie, T., 2001. Kinetic analysis of [^{11}C]MP4A using a high-radioactivity brain region that represents an integrated input function for measurement of cerebral acetylcholinesterase activity without arterial blood sampling. J. Cereb. Blood Flow Metab. 21, 1354–1366.

Namba, H., Iyo, M., Fukushi, K., Shinotoh, H., Nagatsuka, S., Suhara, T., Sudo, Y., Suzuki, K., Irie, T., 1999. Human cerebral acetylcholinesterase activity measured with positron emission tomography: procedure, normal values and effect of age. Eur. J. Nucl. Med. 26, 135–143.

Price, J.C., Klunk, W.E., Lopresti, B.J., Lu, X., Hoge, J.A., Ziolko, S.K., Holt, D.P., Meltzer, C.C., DeKosky, S.T., Mathis, C.A., 2005. Kinetic modeling of amyloid binding in humans using PET imaging and Pittsburgh Compound-B. J. Cereb. Blood Flow Metab. 25, 1528–1547.

Sato, K., Fukushi, K., Shinotoh, H., Nagatsuka, S., Tanaka, N., Aotsuka, A., Ota, T., Shiraishi, T., Tanada, S., Iyo, M., Irie, T., 2004. Evaluation of simplified kinetic analysis for measurement of brain acetylcholinesterase activity using *N*-[^{11}C]methylpiperidine-4-yl propionate and positron emission tomography. J. Cereb. Blood Flow Metab. 24, 600–611.

Schmidt, K., Lucignani, G., Moresco, R.M., Rizzo, G., Gilardi, M.C., Messa, C., Colombo, F., Fazio, F., Sokoloff, L., 1992. Errors introduced by tissue heterogeneity in estimation of local cerebral glucose utilization with current kinetic models of the [^{18}F]fluorodeoxyglucose method. J. Cereb. Blood Flow Metab. 12, 823–834.

Shimada, H., Hirano, S., Shinotoh, H., Aotsuka, A., Sato, K., Tanaka, N., Ota, T., Asahina, M., Fukushi, K., Kuwabara, S., Hattori, T., Suhara, T., Irie, T., 2009. Mapping of brain acetylcholinesterase alterations in Lewy body disease by PET. Neurology 73, 273–278.

Sokoloff, L., Reivich, M., Kennedy, C., Des Rosiers, M.H., Patlak, C.S., Pettigrew, K.D., Sakurada, O., Shinohara, M., 1977. The [^{14}C]deoxyglucose method for the measurement of local cerebral glucose utilization: theory, procedure, and normal values in the conscious and anesthetized albino rat. J. Neurochem. 28, 897–916.

Wong, D.F., Gjedde, A., Wagner Jr., H.N., 1986. Quantification of neuroreceptors in the living human brain. I. Irreversible binding of ligands. J. Cereb. Blood Flow Metab. 6, 137–146.

Wu, Y., Carson, R.E., 2002. Noise reduction in the simplified reference tissue model for neuroreceptor functional imaging. J. Cereb. Blood Flow Metab. 22, 1440–1452.

Cardiac Positron-Emission Tomography Images With an Amyloid-Specific Tracer in Familial Transthyretin-Related Systemic Amyloidosis

Katsutoshi Furukawa, MD, PhD; Shu-ichi Ikeda, MD, PhD; Nobuyuki Okamura, MD, PhD; Manabu Tashiro, MD, PhD; Naoki Tomita, MD, PhD; Shozo Furumoto, PhD; Ren Iwata, PhD; Kazuhiko Yanai, MD, PhD; Yukitsuka Kudo, PhD; Hiroyuki Arai, MD, PhD

We report the case of a 32-year-old man who had suffered from orthostatic syncope and body weight loss since he was 27 years old. As years passed by, he also showed muscle weakness and abnormal sensations in both legs, hyporeflexia in 4 limbs, and autonomic failure (impotence, urinary and fecal incontinence, and edema in lower limbs) suggesting the presence of peripheral somatic and autonomic polyneuropathy. His mother, mother's father, and mother's paternal aunt also had similar symptoms. Both the sensory nerve action potential and the sensory nerve conduction velocity of his right sural nerve were low (1.26 μV and 47.2 m/s, respectively), and the motor nerve conduction velocity of his right tibial nerve was 41.1 m/s (normal >45 m/s). A DNA test on the man disclosed a missense mutation in the transthyretin gene (Ser50Arg), which is relatively rare in familial transthyretin-related systemic amyloidosis.[1,2] Transthyretin-immunoreactive amyloid deposition was demonstrated in the biopsied gastroduodenal mucosa (Figure 1). Echocardiography showed a markedly thickened ventricular wall (thickness of interventricular septum 22.3 mm [normal <12 mm]) with normal wall motion (fractional shortening 37.6% [normal 28–42%]), indicating that he also had cardiac

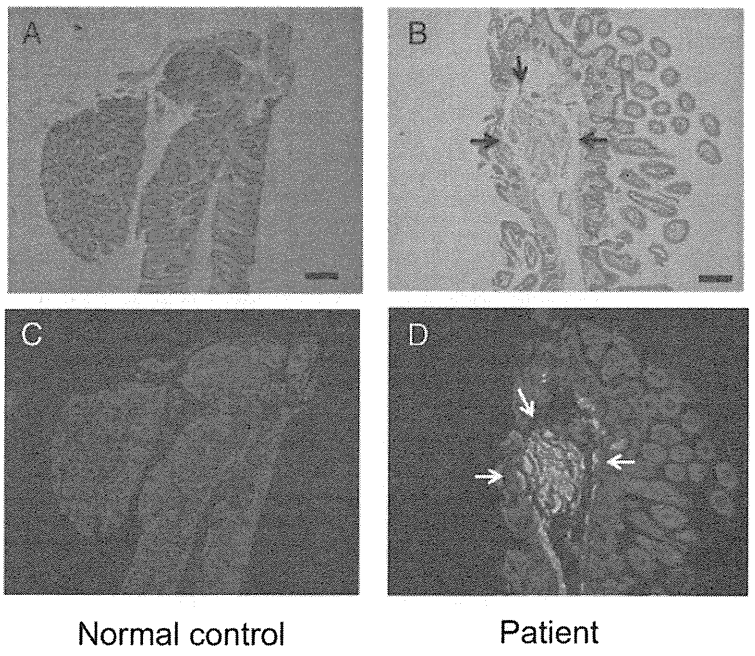

Figure 1. Detection of amyloid deposition in the intestines. Congo red (**A** and **B**) and BF-227 (**C** and **D**) clearly detect transthyretin in the submucosal space of the small intestine of the patient. Scale bars, 100 μm.

From the Department of Geriatrics and Gerontology, Division of Brain Sciences, Institute of Development, Aging and Cancer, Tohoku University (K.F., N.T., H.A.); Department of Medicine (Neurology & Rheumatology), Shinshu University School of Medicine (S.I.); Department of Pharmacology, Tohoku University Graduate School of Medicine (N.O., S.F., K.Y.); Division of Cyclotron Nuclear Medicine, Cyclotron and Radioisotope Center, Tohoku University (M.T.); Division of Radiopharmaceutical Chemistry, Cyclotron and Radioisotope Center, Tohoku University (R.I.); Department of NeuroImaging Research, Innovation New Biomedical Engineering Center, Tohoku University (Y.K.), Sendai, Japan.

Correspondence to Katsutoshi Furukawa, MD, PhD, Department of Geriatrics and Gerontology, Institute of Development, Aging and Cancer, Tohoku University, 4-1 Seiryo-machi Aobaku, Sendai 980-8575 Japan. E-mail kfurukawa-ns@umin.ac.jp

(*Circulation*. 2012;125:556-557.)

Circulation is available at http://circ.ahajournals.org DOI: 10.1161/CIRCULATIONAHA.111.045237

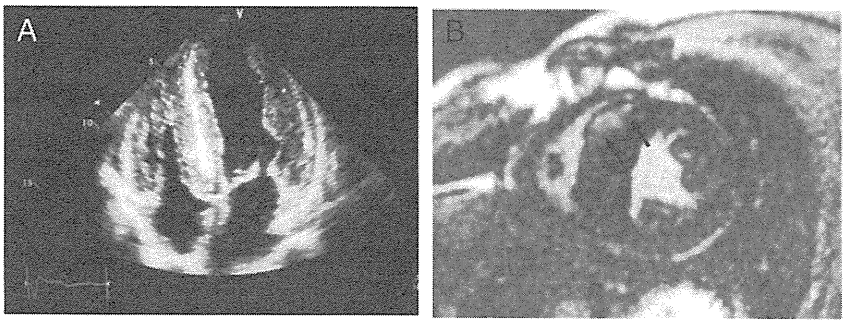

Figure 2. A, Echocardiographic finding. Four chamber views show symmetrical thickening of ventricular walls and septum with hyperrefractile myocardial echo (the so-called granular sparkling appearance). **B**, Contrast magnetic resonance imaging with gadolinium. Focal late gadolinium enhancement is visible (arrows).

amyloidosis (Figure 2A). Contrast magnetic resonance imaging[3] revealed focal late gadolinium enhancement in the thickened ventricular wall (Figure 2B). The patient had been treated with orthotopic live-donor liver transplantation when he was 31 years old to alleviate and prevent exacerbation of his neuronal and cardiac symptoms. His condition, including the neurological disability, gradually improved, and he started to work again 10 months after liver transplantation.

In order to visualize amyloid deposition in the myocardium, the patient underwent a cardiac positron-emission tomography study with [^{11}C]-BF-227 that sensitively and specifically binds to aggregated amyloid fibrils.[4] The positron-emission tomography images revealed significantly robust retention of [^{11}C]-BF-227 in the patient's heart compared with that of the normal control (Figure 3). Biopsy specimens from the patient's duodenum also showed higher signals of BF-227 compared with that of the normal control (Figure 1, C and D). The present result provides evidence that our amyloid-specific positron-emission tomography tracer, [^{11}C]-BF-227, can successfully detect amyloid deposition in the heart. Several molecules, such as ^{99m}Tc-aprotinin and ^{99m}Tc-labeled phosphate derivatives, have been investigated to visualize cardiac amyloidosis.[2] None of the previous tracers, however, could specifically bind to aggregated amyloid, which forms a β-pleated sheet structure. In any of the amyloidgenic disorders, such as transthyretin-related systemic amyloidosis and Alzheimer's disease, it is surmised that the monomer of the amyloid protein itself is not very toxic, whereas misfolded oligomers could cause damage to human organs.[1–4] It is therefore truly important to detect the accumulation of real amyloid fibrils for the early and accurate diagnosis of amyloidosis. To our knowledge, this is the first report showing the usefulness of a β-pleated sheet structure-specific positron-emission tomography in investing visceral organ amyloidosis.

Sources of Funding

This study was supported by the Program for the Promotion of Fundamental Studies in Health Science by the National Institute of Biomedical Innovation; the Special Coordination Funds for Promoting Science and Technology; the Industrial Technology Research Grant Program from the New Energy and Industrial Technology Development Organization of Japan; Health and Labor Sciences Research Grants for Translational Research from the Ministry of Health; and the Ministry of Education, Culture, Sports and Technology of Japan.

Acknowledgments

We appreciate technical assistance of Shoichi Watanuki, Yoichi Ishikawa, Motohisa Kato, and Emiko Fukuda.

Disclosures

None.

References

1. Ikeda S, Nakazato M, Ando Y, Sobue G. Familial transthyretin-type amyloid polyneuropathy in Japan: Clinical and genetic heterogeneity. *Neurology*. 2002;58:1001–1007.
2. Rapezzi C, Quarta CC, Riva L, Longhi S, Gallelli I, Lorenzini M, Ciliberti P, Biagini E, Salvi F, Branzi A. Transthyretin-related amyloidoses and the heart: a clinical overview. *Nat Rev Cardiol*. 2010;7:398–408.
3. Vogelsberg H, Mahrholdt H, Deluigi CC, Yilmaz A, Kispert Eva M, Greulich S, Klingel K, Kandolf R, Sechtem U. Cardiovascular magnetic resonance in clinically suspected cardiac amyloidosis. *J Am Coll Cardiol*. 2008;s51:1022–1030.
4. Furukawa K, Okamura N, Tashiro M, Waragai M, Furumoto S, Iwata R, Yanai K, Kudo Y, Arai H. Amyloid PET in mild cognitive impairment and Alzheimer's disease with BF-227: Comparison to FDG-PET. *J Neurol*. 2010;257:721–727.

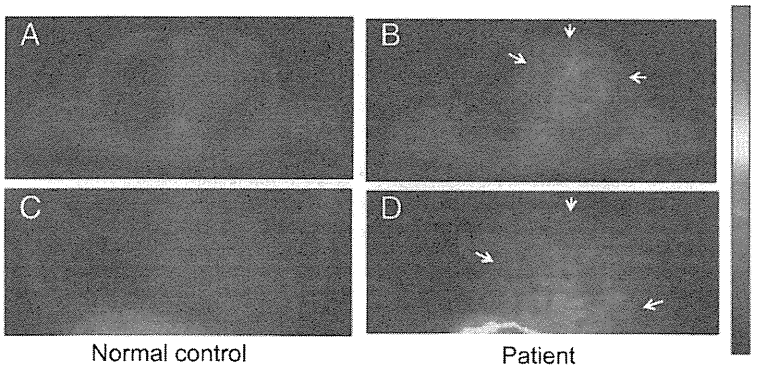

Figure 3. [^{11}C]-BF-227 positron emission tomgraphy succeeds in visualization of amyloid deposition in the heart. Axial and coronal images are **A** and **B** and **C** and **D**, respectively. Arrows indicate high signals of [^{11}C]-BF-227 in the heart of the patient (**B** and **D**).

Ann Nucl Med (2011) 25:732–739
DOI 10.1007/s12149-011-0518-7

ORIGINAL ARTICLE

A modified method of 3D-SSP analysis for amyloid PET imaging using [^{11}C]BF-227

Tomohiro Kaneta · Nobuyuki Okamura · Satoshi Minoshima · Katsutoshi Furukawa · Manabu Tashiro · Shozo Furumoto · Ren Iwata · Hiroshi Fukuda · Shoki Takahashi · Kazuhiko Yanai · Yukitsuka Kudo · Hiroyuki Arai

Received: 23 March 2011 / Accepted: 6 July 2011 / Published online: 27 July 2011

Abstract
Objective Three-dimensional stereotactic surface projection (3D-SSP) analyses have been widely used in dementia imaging studies. However, 3D-SSP sometimes shows paradoxical results on amyloid positron emission tomography (PET) analyses. This is thought to be caused by errors in anatomical standardization (AS) based on an ^{18}F-fluorodeoxyglucose (FDG) template. We developed a new method of 3D-SSP analysis for amyloid PET imaging, and used it to analyze ^{11}C-labeled 2-(2-[2-dimethylaminothiazol-5-yl]ethenyl)-6-(2-[fluoro]ethoxy)benzoxazole (BF-227) PET images of subjects with mild cognitive impairment (MCI) and Alzheimer's disease (AD).
Methods The subjects were 20 with MCI, 19 patients with AD, and 17 healthy controls. Twelve subjects with MCI were followed up for 3 years or more, and conversion to AD was seen in 6 cases. All subjects underwent PET with both FDG and BF-227. For AS and 3D-SSP analyses of PET data, Neurostat (University of Washington, WA, USA) was used. Method 1 involves AS for BF-227 images using an FDG template. In this study, we developed a new method (Method 2) for AS: First, an FDG image was subjected to AS using an FDG template. Then, the BF-227 image of the same patient was registered to the FDG image, and AS was performed using the transformation parameters calculated for AS of the corresponding FDG images. Regional values were normalized by the average value obtained at the cerebellum and values were calculated for the frontal, parietal, temporal, and occipital lobes. For statistical comparison of the 3 groups, we applied one-way analysis of variance followed by the Bonferroni post hoc test. For statistical comparison between converters and non-converters, the t test was applied. Statistical significance was defined as $p < 0.05$.

T. Kaneta (✉) · S. Takahashi
Department of Diagnostic Radiology,
Tohoku University, 1-1 Seiryomachi, Aobaku,
Sendai 980-8574, Japan
e-mail: kaneta@rad.med.tohoku.ac.jp

N. Okamura · S. Furumoto · K. Yanai
Department of Pharmacology, Tohoku University Graduate School of Medicine, 4-1 Seiryomachi,
Aobaku, Sendai 980-8575, Japan

S. Minoshima
Department of Radiology, University of Washington,
1959 N.E. Pacific Street, Seattle, WA 98195-7115, USA

K. Furukawa · H. Arai
Division of Brain Sciences, Department of Geriatrics and Gerontology, Institute of Development, Aging and Cancer,
Tohoku University, 4-1 Seiryomachi, Aobaku,
Sendai 980-8498, Japan

M. Tashiro
Division of Cyclotron Nuclear Medicine, Cyclotron and Radioisotope Center, Tohoku University, 6-3 Aoba,
Aramaki, Aoba-ku, Sendai, Miyagi 980-8578, Japan

R. Iwata
Division of Radiopharmaceutical Chemistry, Cyclotron and Radioisotope Center, Tohoku University, 6-3 Aoba, Aramaki,
Aoba-ku, Sendai, Miyagi 980-8578, Japan

H. Fukuda
Nuclear Medicine and Radiology, Institute of Development,
Aging and Cancer, Tohoku University, 4-1 Seiryomachi,
Aobaku, Sendai 980-8498, Japan

Y. Kudo
Department of NeuroImaging Research, Innovation New Biomedical Engineering Center, Tohoku University,
4-1 Seiryomachi, Aobaku, Sendai 980-8498, Japan

Results Among the 56 cases we studied, Method 1 demonstrated slight distortions after AS of the image in 16 cases and heavy distortions in 4 cases in which the distortions were not observed with Method 2. Both methods demonstrated that the values in AD and MCI patients were significantly higher than those in the controls, in the parietal, temporal, and occipital lobes. However, only Method 2 showed significant differences in the frontal lobes. In addition, Method 2 could demonstrate a significantly higher value in MCI-to-AD converters in the parietal and frontal lobes.

Conclusions Method 2 corrects AS errors that often occur when using Method 1, and has made appropriate 3D-SSP analysis of amyloid PET imaging possible. This new method of 3D-SSP analysis for BF-227 PET could prove useful for detecting differences between normal groups and AD and MCI groups, and between converters and non-converters.

Keywords 3D-SSP · Voxel-based · Amyloid · PET · BF-227

Introduction

Three-dimensional stereotactic surface projection (3D-SSP) analysis [1, 2] has been widely used in dementia imaging studies. This is a method of analysis that extracts metabolic activity from cortical gray matter after anatomical standardization (AS). By extracting the peak activity for each corresponding area of the cortex and assigning it to a surface pixel, the algorithm also can compensate for individual differences in cortical thickness and gyri depth in the standard stereotactic system. Thus, 3D-SSP is advantageous in intergroup comparisons and provides sensitive and robust results when evaluating dementing diseases [2]. However, 3D-SSP sometimes demonstrates paradoxical results on amyloid PET analyses, such as significant abnormalities in cognitively normal subjects. This is thought to be caused by AS errors. Automated AS requires a digital brain template that is matched anatomically with a standard brain atlas. 3D-SSP uses a brain template created by averaging a large number of normal ^{18}F-fluorodeoxyglucose (FDG) positron emission tomography (PET) data (FDG template) [1]. FDG accumulates mainly in the gray matter in the brain, thus showing a totally different distribution from the amyloid PET tracer. On the other hand, amyloid PET tracers, such as Pittsburgh Compound-B (PiB) [3, 4] and ^{11}C-labeled 2-(2-[2-dimethylaminothiazol-5-yl]ethenyl)-6-(2-[fluoro]ethoxy)benzoxazole (BF-227) [5, 6], often demonstrate non-specific high levels of accumulation in the white matter, more commonly in cognitively normal individuals. The FDG template therefore seems inappropriate for 3D-SSP analysis of amyloid PET images. However, a template for amyloid PET is not yet available for 3D-SSP analysis. In this study, we report the development of a new 3D-SSP analysis method for amyloid PET imaging, which solves this problem; we also describe its use in the analysis of BF-227 PET in normal subjects as well as patients with mild cognitive impairment (MCI) and Alzheimer's disease (AD).

Methods

Subjects recruited in the present study included 20 individuals with amnestic MCI, 19 patients with AD, and 17 age-matched normal controls (NC). The demographic parameters of the subjects are shown in Table 1. Among the MCI subjects, 12 were followed up for 3 years or more, and conversion to AD was seen in 6. The control group was recruited from among volunteers, none of whom were on centrally acting medication, had cognitive impairment, or had cerebrovascular lesions identified on MRI. The study protocol was approved by the Committee on Clinical Investigation at Tohoku University School of Medicine and the Advisory Committee on Radioactive Substances at Tohoku University. After describing the study to the patients and subjects, written informed consent was obtained.

All subjects underwent PET with both FDG and BF-227. BF-227 and its *N*-desmethylated derivative (a precursor of BF-227) were custom-synthesized by Tanabe R&D Service Co. BF-227 was synthesized from the precursor by *N*-methylation in dimethyl sulfoxide using [^{11}C]methyl triflate. Both FDG and BF-227 PET were performed using a PET SET-2400W scanner (Shimadzu Inc., Japan) with a spatial resolution of 4 mm (transaxial) and 4.5 mm (axial) at full-width half-maximum (FWHM) in the center of the field of view. For attenuation correction, a transmission scan was performed using ^{68}Ge/Ga sources for 7 min. The BF-227 PET scan was performed for 60 min after intravenous injection of 211–366 MBq of BF-227 with the subjects' eyes closed. The data obtained at 40–60 min after injection were used for the calculation of standardized uptake value (SUV), a tissue radioactivity concentration

Table 1 Demographic details of the subjects in this study

	N	Gender	Age	MMSE
NC	17	M/F = 7/10	67.0 ± 4.1	29.9 ± 0.3
MCI	20	M/F = 10/10	76.6 ± 4.7	25.5 ± 2.3
AD	19	M/F = 5/14	73.7 ± 7.0	20.0 ± 3.5

NC normal control, *MCI* mild cognitive impairment, *AD* Alzheimer's disease, *M* male, *F* female

normalized by injected dose and body weight. For FDG PET, subjects were scanned after at least 4 h of food restriction in a quiet and dimly lit room with their eyes closed. An emission scan was performed 60 min after intravenous injection of about 370 MBq of FDG for 10 min. The emission data were corrected for tissue attenuation on the basis of the transmission data.

Anatomical standardization of BF-227 images

Two kinds of AS for BF-227 images were performed: (1) Method 1, which performs AS for BF-227 images using an FDG template; (2) Method 2 (a new method for AS), which we have described below. First, the FDG image was subjected to AS using an FDG template. The BF-227 image was then registered to the FDG image, and AS was performed using the transformation parameters calculated for AS of the corresponding FDG images. We used the software library Neurostat (University of Washington, Seattle, WA, USA) for neurological and biomedical image analyses. The programs used in Method 2 were mainly "stereo," "coreg," and "swarpreg." "Stereo" is a program for stereotactic image registration, and creates library files containing data for linear and nonlinear transformation. In Method 2, we created these library files for FDG images, and applied them to BF-227 images. "Coreg" is a program for three-dimensional image co-registration, which we used to align BF-227 images to FDG images. Next, we used "swarpreg," which is a program for three-dimensional stereotactic image warping for BF-227 images that uses library files for FDG images. A combination of these procedures enabled the transformation of individual BF-227 images into the stereotactic space of the standard brain.

Analysis

Regional values were extracted from cortical gray matter to the surface of the template by the 3D-SSP method in the same manner as FDG PET, and were normalized by the extracted value from the cerebellar gray matter (eSUVR). The values were calculated for the frontal, parietal, temporal, and occipital lobes using "sspvoiclassic" program in Neurostat. The right and left lobes of each subject were analyzed evenly. For statistical comparison between the 3 groups, we applied one-way analysis of variance followed by the Bonferroni post hoc test. For statistical comparison between converters and non-converters, the t test was applied. Statistical significance was defined as $p < 0.05$.

For voxel-based comparison with normal subjects, normal databases were created by averaging the images from NC after AS by Method 1 and 2, individually. The 3D-SSP z-map images were normalized to those of the cerebellum, and were shown within the range of 1–5 of the z score.

For voxel-based two-sample comparison, t test was applied. Z scores were calculated using "ssp2tz" program in Neurostat. The 3D-SSP z-map images were shown within the range of 1–5 of the z score.

Results

Case presentation

The patient was an 81-year-old woman with a diagnosis of MCI. The mini-mental state examination (MMSE) score was 26. FDG PET did not demonstrate an AD-like pattern, which is characterized by decreased uptake at the parietal lobe or posterior cingulate gyrus (Fig. 1a). BF-227 PET did not demonstrate significantly increased uptake in the brain (Fig. 1b). However, 3D-SSP results analyzed by Method 1 showed significant generalized abnormalities in the brain, suggesting AD (Fig. 1c). On the other hand, those analyzed by Method 2 did not demonstrate such abnormalities (Fig. 1d). This patient was followed up for over 3 years, but did not convert to AD. Figure 1e shows the BF-227 image after AS by Method 1, showing considerable distortions, mainly in the frontal lobes. The BF-227 image after AS by Method 2 did not show such distortions (Fig. 1f).

Anatomical standardization

When a total of 56 cases were analyzed by both methods, Method 1 demonstrated 17 cases with slightly distorted images and 4 cases with heavily distorted images after AS. Table 2 shows the cases with such distortions after Method 1. These distortions were mainly seen at the frontal lobes with angular deformity, and were seen uniformly among subjects with AD, MCI, and NC. On the other hand, analysis by Method 2 did not show such distortions, and AS was successful in these cases (Fig. 1). However, scan failure in one case and an error in the registration of the BF-227 image to the FDG image in another case necessitated their exclusion from subsequent analyses.

Regional analyses

The regional analyses demonstrated that the mean values for the AD, MCI, and NC groups by Method 1 were in the range 1.05–1.09, 1.01–1.05, and 0.96–0.98, respectively, while they were found to be 1.08–1.12, 1.06–1.10, and 0.96–1.00, respectively, by Method 2. Method 2 demonstrated significant differences between AD and NC, and